ENERGY TRANSFER ENHANCEMENT OF PHOTON UPCONVERSION SYSTEMS FOR SOLAR ENERGY HARVESTING

A Thesis
Presented to
The Academic Faculty

by

Ji-Hwan Kang

In Partial Fulfillment
of the Requirements for the Degree
Master of Science in the
School of Chemical and Biomolecular Engineering

Georgia Institute of Technology
December 2012

ENERGY TRANSFER ENHANCEMENT OF PHOTON UPCONVERSION SYSTEMS FOR SOLAR ENERGY HARVESTING

Approved by:

Dr. Elsa Reichmanis, Advisor
School of Chemical and Biomolecular Engineering
Georgia Institute of Technology

Dr. Dennis W. Hess
School of Chemical and Biomolecular Engineering
Georgia Institute of Technology

Dr. William J. Koros
School of Chemical and Biomolecular Engineering
Georgia Institute of Technology

Date Approved: 26th September 2012

ACKNOWLEDGEMENTS

First, I wish to express my sincere appreciation to my advisor, Prof. Elsa Reichmanis, for all of her strong support. She has always encouraged me whenever I was in trouble with any academic or research problems so that I could continue my work without frustration. I would also like to thank my committee, Prof. Dennis Hess and Prof. William Koros, who have advised me in this work. They allowed me to broaden my perspective and contribute to my personal development by expanding my knowledge with high level of completion.

I wish to thank most sincerely the research group members, Dr. Zhaokang Hu, Dr. Avishek Aiyar, Mincheol Chang, Boyi Fu, Dalsu Choi, and Nabil Kleinhenz for their valuable help and support. I also give many thanks to Candice Porter who joined our laboratory as a REU (research experiences for undergraduates) student during the summer of 2012. At that time, I had a wonderful experience by having a mentor/mentee relationship with her and was strongly motivated by her. And I appreciate Andrew Shaw who is primary manager of the confocal laboratory. I have gained experience in confocal microscopy from him because he was always willing to help me further understand the capabilities and results through many discussions.

Finally, I would like to express my sincere gratitude to my family for their continuous support and encouragement, especially my wife, Sowon, for her love and faith in me and her understanding. It is to her and to our son and daughter, Insung & Heesung, that this work is dedicated.

TABLE OF CONTENTS

LIST OF TABLES

Page

LIST OF FIGURES

Page

SUMMARY

Photon energy upconversion (UC), a process that can convert two or more photons with low energy to a single photon of higher energy, has the potential for overcoming the thermodynamic efficiency limits of sunlight-powered devices and processes. An attractive route to lowering the incident power density for UC lies in harnessing energy transfer through triplet-triplet annihilation (TTA). To maximize energy migration in multicomponent TTA-assisted UC systems, triplet exciton diffusivity of the chromophores within an inert medium is of paramount importance, especially in a solid-state matrix for practical device integration.

In this thesis, low-threshold sensitized UC systems were fabricated and demonstrated by a photo-induced interfacial polymerization within a coaxial-flow microfluidic channel and in combination with nanostructured optical semiconductors. Dual-phase structured uniform UC capsules allow for the highly efficient bimolecular interactions required for TTA-based upconversion, as well as mechanical strength for integrity and stability. Through controlled interfacial photopolymerization, diffusive energy transfer-driven photoluminescence in a bi-molecular UC system was explored with concomitant tuning of the capsule properties. We believe that this core-shell structure has significance not only for enabling promising applications in photovoltaic devices and photochromic displays, but also for providing a useful platform for photocatalytic and photosensor units.

Furthermore, for improving photon upconverted emission, a photonic crystal was integrated as an optical structure consisting of monodisperse inorganic colloidal nanoparticles and polymer resin. The constructively enhanced reflected light allows for the reuse of solar photons over a broad spectrum, resulting in an increase in the power conversion efficiency of a dye-sensitized solar cell as much as 15-20 %.

CHAPTER 1

INTRODUCTION

1.1. Photon energy upconversion

Photon energy upconversion (UC), the generation of higher energy photons than that of the incident light, is a promising optical process due to its potential applications in photosensitive devices, including photovoltaics,[1-5] photocatalyst systems,[6-8] photochromic displays,[9,10] and biological imaging,[11-14] as shown in Figure 1.1. However, conventional UC systems based upon nonlinear phenomena such as two-photon absorption and second-harmonic generation require high excitation intensities (in the range of megawatt per square centimeter), and as a result may be undesirable.[15] An attractive alternative approach uses a triplet-triplet annihilation (TTA) based process which allows the use of low-power density (in the range of milliwatt per square centimeter) noncoherent continous-wave excitation, e.g. sunlight (100 $mWcm^{-2}$, AM 1.5G).[16-19] Although sensitized TTA UC was first introduced by Parker and Hatchard in the early 1960's,[20,21] this phenomenon was only sparingly investigated over the subsequent decades because their noncovalent organic systems whose triplet sensitizers exhibited low intersystem crossing yielded only limited upconverted fluorescence efficiency. However recently, many research groups have demonstrated that the incorporation of metal-organic chromophores can markedly enhance upconversion yield since the sensitizer triplet state can be populated with high efficiency upon absorption of light.[15,16] Most recently, this UC method was integrated into a solar cell to overcome the theoretical power efficiency limit.[4,22] The TTA approach typically uses an organometallic complex and an aromatic hydrocarbon as the sensitizer (donor) and emitter (acceptor), respectively. The metal-to-ligand charge-trasfer (MLCT) characteristics of the sensitizer

enables its long-lived triplet excited state by enhancing the intersystem crossing (ISC) rate,[23] resulting in triplet-triplet energy transfer (TTET) to the acceptor. Two triplet excited acceptor molecules then undergo TTA through direct collision and subsequent generation of one singlet excited state, which produces the upconverted fluorescence upon decay to the ground state.

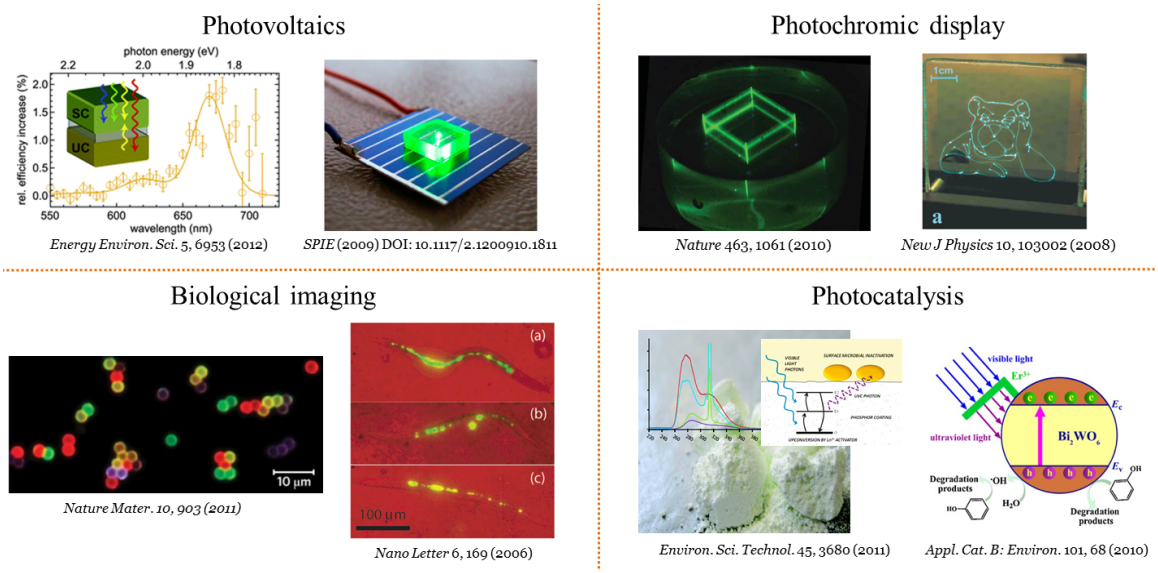

Figure 1.1. Potential application fields of photon energy upconversion.[1-4,6-14]

1.2. Requirements for TTA-based photon upconversion

The sensitized TTA mechanism involves the transfer of energy between a donor and an acceptor. Hence, several factors are considered when determining the proper combination of chromophores in a viable upconverting system.[10] A schematic representation of the process of photon energy upconversion based on TTA in a multi-molecular system is shown in Figure 1.2. After long wavelength selective excitation of the sensitizer, TTA must be considered as an inherently connected chain of three processes (Figure 1.3). The first process in the chain is the ISC, which is strongly enhanced by spin-orbit coupling to the metal center of metallated macrocyclic sensitizer molecules. Efficient ISC within the sensitizer molecules ensures a high population of the

sensitizer triplet level via single photon absorption. On other hand, the very weak ISC of the emitter molecules substantially prohibits the depopulation of the excited emitter triplet states via phosphorescence and thus preserves the created triplet population of the emitter for the process of TTA. Therefore, a large difference between the ISC coefficients of the sensitizer and emitter molecules is required ($C^{ISC}_{sensitizer} >> C^{ISC}_{emitter}$). The second process in the chain is energy transfer of the excitation of the sensitizer triplet to the emitter triplet (TTET). The efficiency of the TTET is predetermined by the extent of overlap of the sensitizer and emitter triplet manifolds ($E^{triplet*}_{sensitizer} >\cong E^{triplet*}_{emitter}$). The third process is the subsequent TTA. As a precondition for efficient energetically conjoined TTA-UC, there are two requirements related to the molecular structure of the sensitizer and the emitter molecules. The combined triplet energy level from two excited emitter molecules is greater than or equal to the first excited singlet state of the emitter molecule without using thermal energy ($2E^{triplet*}_{emitter} \geq E^{singlet*}_{emitter}$). The final requirement for the UC system relates to the structure of the sensitizer absorption spectrum. In order to reduce the re-absorption of the generated UC emission from sensitizer molecules which are in the ground state, there should be a large enough transparent window. Metallated macrocycles such as porphyrins have band-like absorption spectra grouped around two strong bands, which are the Soret- and Q-bands. Therefore, photons with energies lying sufficiently far away from those two absorption maxima will be absorbed less by a sensitizer molecule, and the position of the first excited singlet state level of the emitter should not overlap with the absorption maxima of the sensitizer ($E^{Soret-band}_{sensitizer} > E^{singlet*}_{emitter} >> E^{Q-band}_{sensitizer}$). As long as these specific energy criteria are met, then conditions are appropriate for the observation of anti-Stokes upconverted fluorescence from the sample as shown in Figure 1.4.

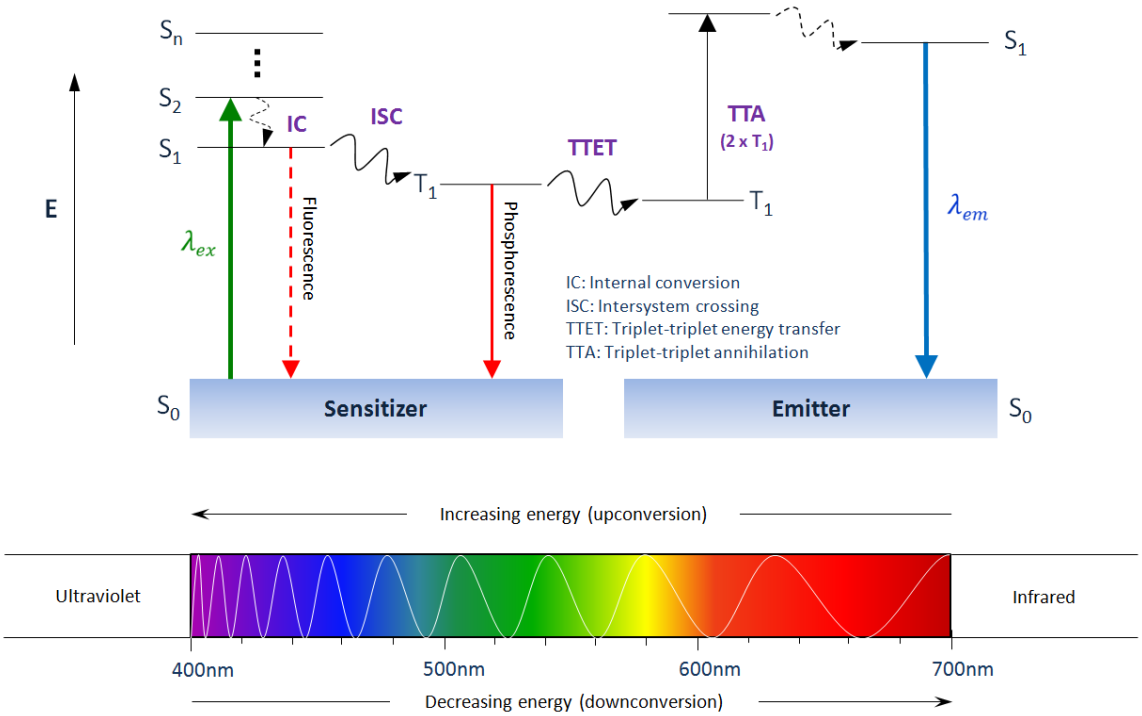

Figure 1.2. Generalized energy level diagram of the photon energy upconversion process via sensitized triplet-triplet annihilation leading to the singlet delayed fluorescence. Colored solid lines represent possible radiative processes.

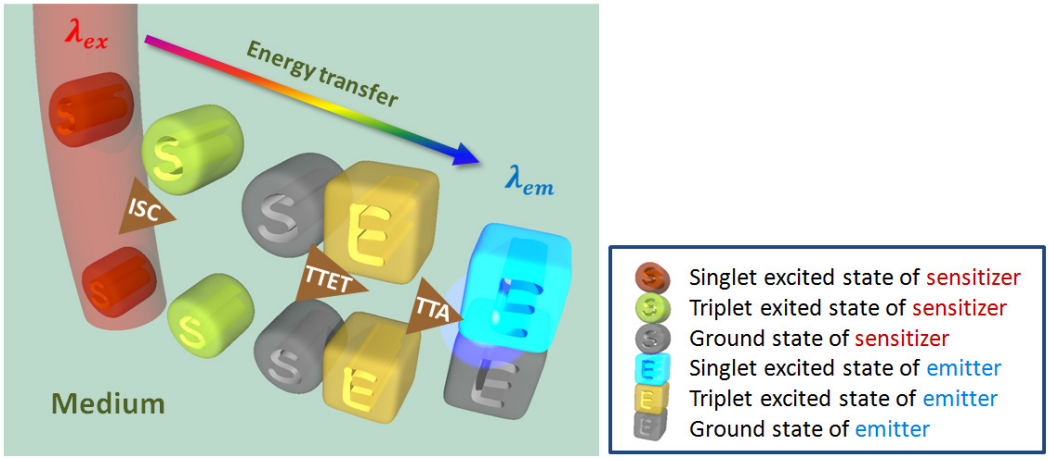

1) ISC $2^1S^* \rightarrow 2^3S^*$

2) TTET $2(^3S^* + E^0) \rightarrow 2(S^0 + {}^3E^*)$

3) TTA $^3E^* + {}^3E^* \rightarrow {}^1S^* + S^0$

Figure 1.3. Inherently connected chain of three processes for triplet-triplet assisted photon energy upconversion.

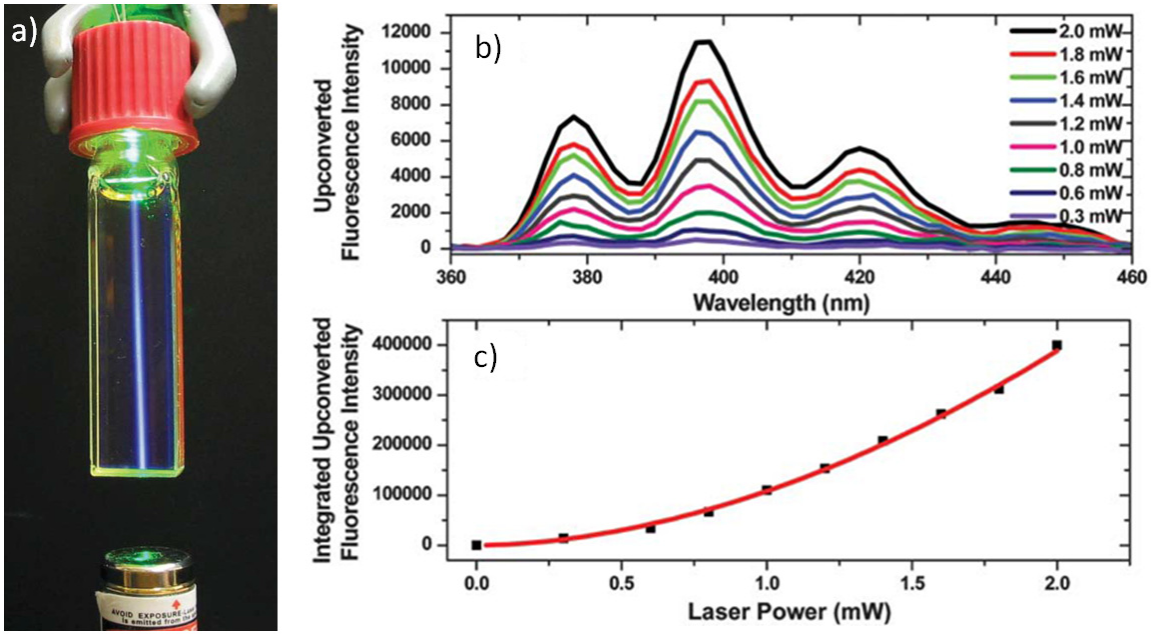

Figure 1.4. TTA-assisted anti-Stokes upconverted fluorescence: (a) Digital photograph of upconverted fluorescence produced in 4:1 toluene-acetonitrile solutions of $[Ru(dmb)_3]^{2+}$ and DPA. Excitation by a commercial green laser pointer (< 5 mW, 532 nm), (b) Upconverted fluorescence intensity profile of a deaerated acetonitrile solution of $[Ru(dmb)_3]^{2+}$ and DPA as a function of 514.5 nm incident laser power. (c) Integrated emission intensity from part (b) represented as black squares. The solid red line is the best quadratic fit to the integrated emission data.[24]

Sensitizers are selected based on their ability to absorb light in the visible-to-near-IR region of the spectrum allowing for low energy excitation and many possess a relatively long triplet excited state lifetime, typically on the order of several microseconds and beyond. This latter requirement is necessary to facilitate conditions enabling efficient diffusion-based quenching. Metallated sensitizers that exhibit MLCT excited states as well as heavy metal-containing porphyrins and phtalocyanines have been generally studied since the presence of the π-conjugated aromatic rings shifts their respective absorption and emission maxima towards the red and near-IR region of the spectrum and the heavy metal strongly enhances the spin-orbit coupling which yields ISC efficiencies near unity.

To date, the majority of the sensitized UC studies have been carried out in deoxygenated solution at room temperature. In order to fully exploit the upconversion

process, however, it would be highly attractive if solid materials could be developed that were capable of displaying this effect for potential device integration. This advance would, for example, permit the utilization of wavelength-shifting films in combination with solid-state lasers, or in photovoltaics, enabling more complete harnessing of the solar spectrum. Ultimately, this is particularly valuable for making better use of the near-IR region in real devices. With the notion that chromophore diffusion must be possible to allow for the energy transfer of two triplets in low-concentration dye/polymer blends, copolymers such as ethyleneoxide and epichlorohydrin (EO-EPI) and poly(urethane) have served as examples of rubbery polymer host matrices as shown in Figure 1.5. However, translational mobility of the chromophores in the matrix polymer was completely suppressed below the glass transition temperature and even partially suppressed at the room temperature, preventing the necessary bimolecular interaction between donor and acceptor required for TTET and between two acceptor/annihilator molecules required for TTA (Figure 1.6). These observations are qualitatively consistent with sequential bimolecular chemical steps under diffusion control as predicted by the Stokes-Einstein relationship ($D = kT / 6\pi\eta R$ **)** where the chromophore diffusion coefficients (D) are directly proportional to the temperature (T) and inversely proportional to the viscosity (η) of the medium. Therefore, the overall upconverting efficiency was determined by these cooperative effects which promote fast diffusion and more efficient energy transfer collisions rending improved upconversion yields as shown in Figure 1.7. The lower observed quantum efficiency reported in the solid state was proposed to be a result of low triplet exciton mobility and hence it was concluded that a polymer host with an increased diffusion coefficient needs to be considered.

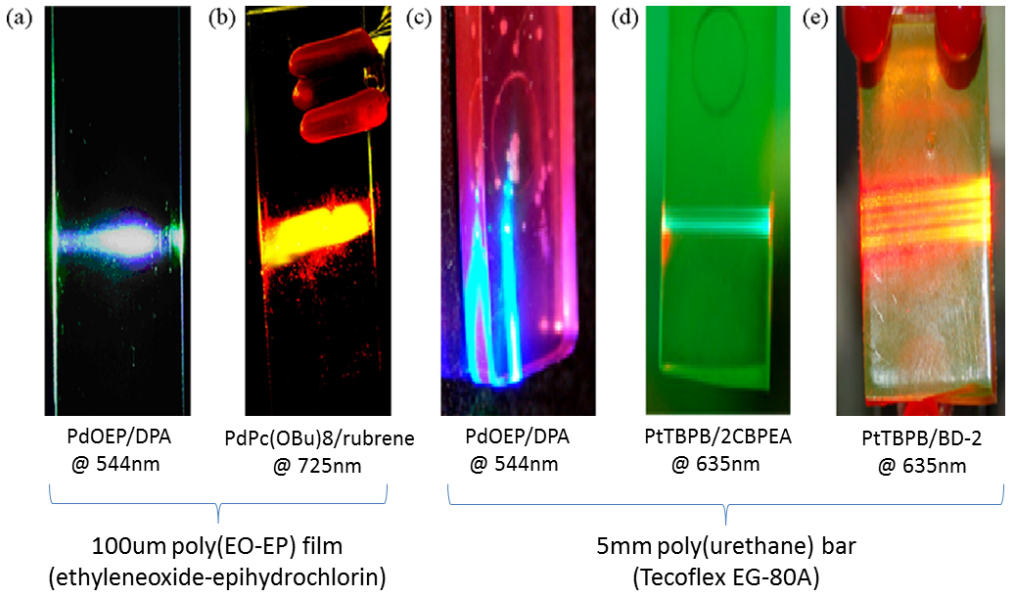

Figure 1.5. Selectively excited photon upconversion systems in rubbery polymers.[16]

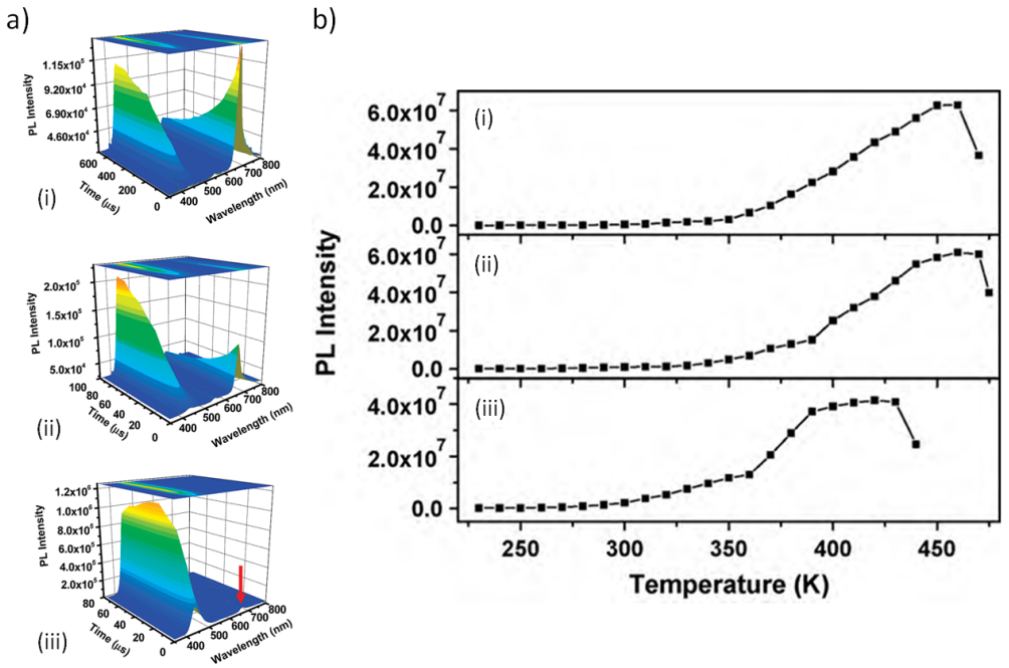

Figure 1.6. Upconverted PL intensity as a function of temperature in various rubbery polymers: (a) Time-resolved emission spectra of an EO-EPI polymer film containing PdOEP (sensitizier) and DPA (emitter) under vacuum measured at (i) 292 K, (ii) 320 K, and (iii) 360 K (red arrow displays the phosphorescence of PdOEP.), following 7 ns, 544±2 nm, 2 mJ Nd:YAG/OPO laser system. (b) Upconverted PL intensity as a function of temperature obtained from PdOEP/DPA doped films of (i) Texin 270, (ii) Texin 285, and (iii) Tecoflex EG-80A.[5]

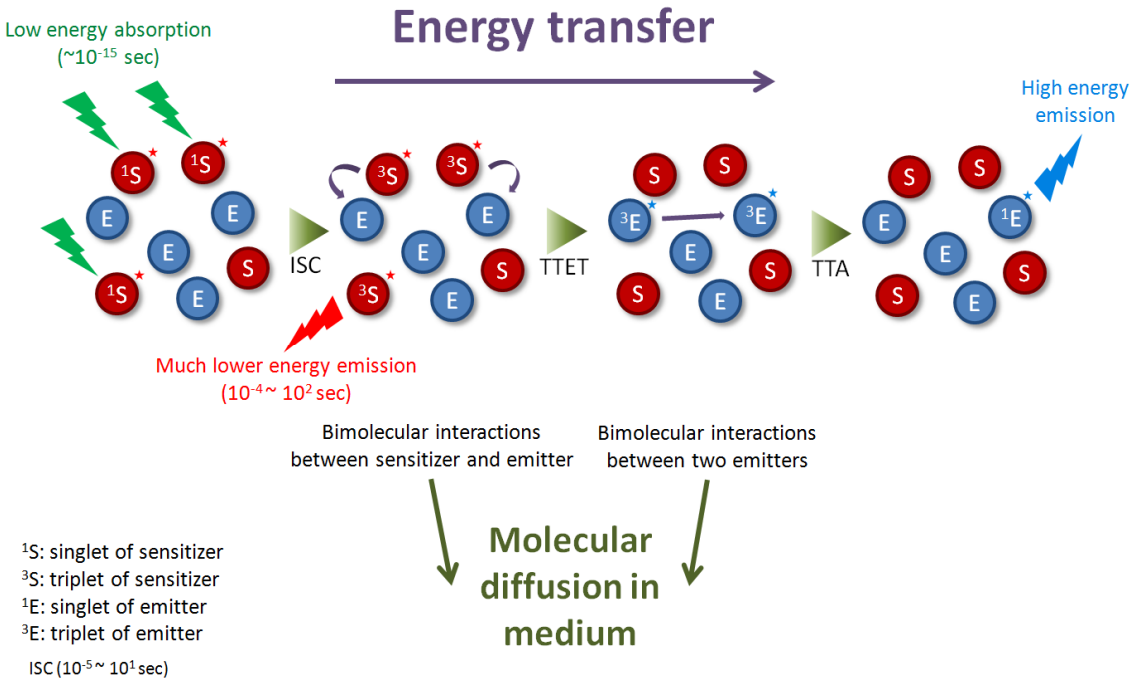

Figure 1.7. Sandwiched state model of photon upconverting energy transfer dependant on molecular diffusive collision in a medium.

1.3. Photonic crystal structures

As shown in Figure 1.8, photonic crystals (PhCs) which consist of regular repeating interval regions with different dielectric constants have a band gap that prohibits transmission of a certain wavelength of light.[25] They are found easily in various forms in nature. Opals and morpho butterflies are two examples.

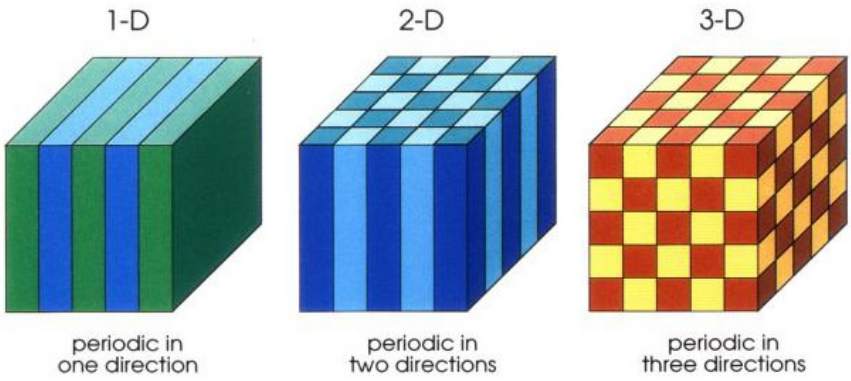

Figure 1.8. Examples of one-, two-, and three-dimensional photonic crystals.[26]

For the first, Yablonovitch suggested that full three-dimensional dielectric structures with periodicity of $\lambda/2$ can lead to the inhibition of spontaneous emission, not being able to propagate near the wavelength λ irrespective of direction.[27,28] Since PhC was proposed, much interest and attention has been focused on studies related to the control of light. Because it can create a forbidden gap in the electromagnetic spectrum like a semiconducting material with electronic band gap, photons will be replaced with electrons to improve the progress of integrated systems with high-density such as optoelectronic and optofluidic device.[29] Therefore, PhCs which are able to manipulate light will have potential future applications in optical integrated circuits.

1.4. Photonic bandgap of photonic crystals

For a constant refractive index, an electromagnetic wave (i.e. light) can be obtained by the dispersion relation, which gives[30]

$$w = (c/n)k$$

,where w is the angular frequency ($w = 2\pi f$), c is the velocity of light, n is the refractive index, and k is the wave number ($k = 2\pi/\lambda$). Figure 1.9 shows that frequency (f) regarding wavelength of light (λ) is always a linear function in vacuum or a medium with constant refractive index, while there are frequency regions in periodic dielectric media where propagating photons are not permitted and the dispersion relation is no longer linear. In other words, if light with a frequency corresponding to the discontinuous regions enters the regular dielectric structure vertically, it cannot pass through and be reflected perfectly.[31] In particular, a range of omni-directional prohibited wavelengths in a 3D PhC means that it has a completely full-photonic band gap.

Due to physical periodic dielectric variations in a PhC, a band gap is opened by splitting the degeneracy at $k = \pm\pi/a$ in the irreducible Brillouin-zone boundaries, and Bragg's condition is satisfied when λ is equal to $2a$.[32] Two dispersion lines of

$\cos(\pi x / a)$ and $\sin(\pi x / a)$ standing waves form the lower and upper edges of the band gap (Figure 1.10). Because these two waves have the same wavelength at different refractive indices, they have different frequencies. The former state concentrated in the higher index (n_{high}) has lower frequency than the latter.[33] Therefore, the photonic band gap width can be related to the refractive index contrast.

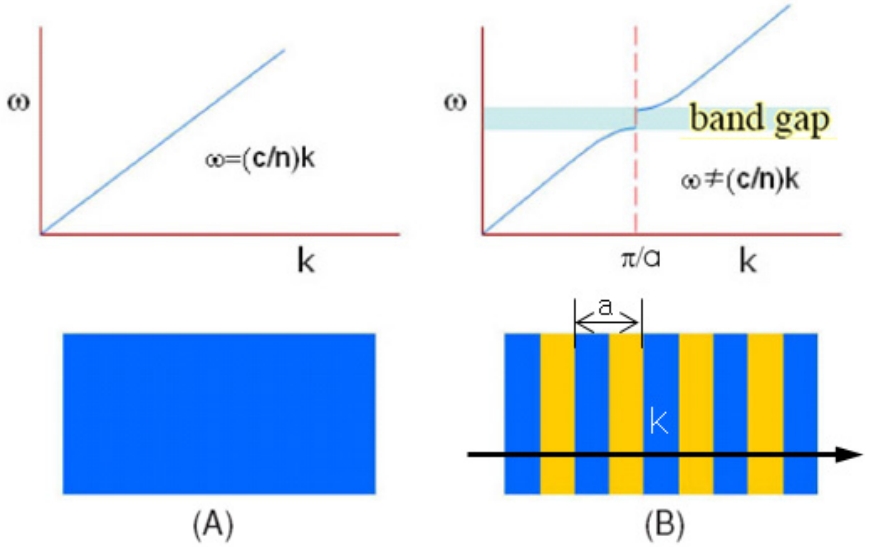

Figure 1.9. Energy dispersion relations of wave vector and angular frequency for (a) a free photon in vacuum (or medium with constant refractive index) and (b) a photon in 1-D photonic crystal.

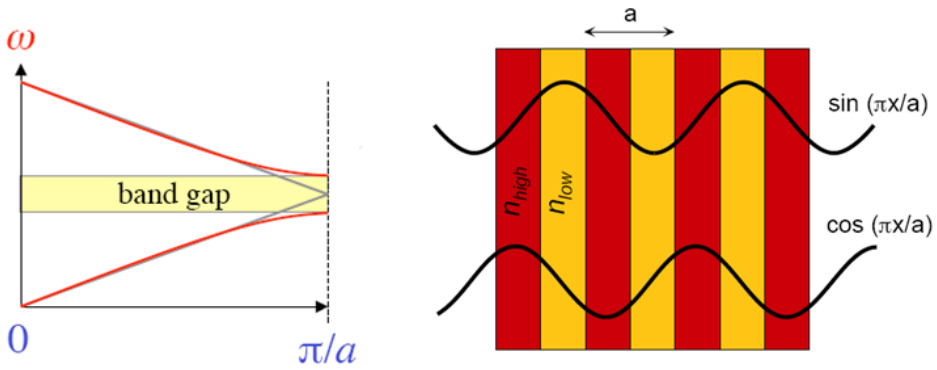

Figure 1.10. Origin of the band gap in 1-D photonic crystal. Two split modes of standing waves by a dielectric periodicity, forming the lower and upper edges of the band gap, respectively.[32,34]

All of electromagnetism, including the propagation of the light in a PhC, are governed by Maxwell's equations.[26] The dispersion relation of photonic band gaps can be predicted exactly by solving Maxwell's equations under the periodic boundary condition. As an expedient to avoid using complex numerical analysis, Bragg's law can also provide for simple estimation in a one-dimensional periodic structure (Figure 1.11). As a result of the diffraction analysis of light, the interference is constructive when the phase shift is a multiple to 2π . The equation satisfying this condition can be expressed by Bragg's law, which originated from experiments related to the diffraction of X-rays or neutrons from surfaces of periodic crystal at a given angle.

$$m\lambda = 2d\sin\theta$$

,where m is an integer determined by the order given, λ is the wavelength of reflected light, d is the spacing between the planes in the lattice, and θ is the angle between the incident light and the plane.

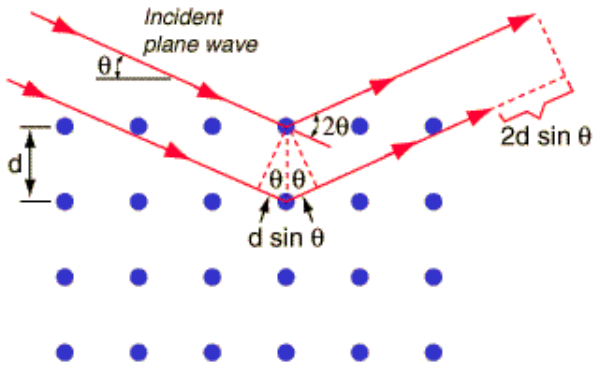

Figure 1.11. Constructive interference condition of Bragg's law.

To control the forbidden wavelength of light, desired PhCs can be designed via photonic band gap engineering where technology innovation is accomplished by tuning proper structural relations between contrast of refractive index and lattice constant or interval (i.e. periodicity of dielectric structure).

CHAPTER 2

EXPERIMENTAL METHODS

2.1. Chemicals and Materials

For one example of the chromophore pairs used to demonstrate triplet-triplet annihilation based photon energy upconversion, Platinum(II)-tetraphenyl Tetrabenzoporphyrin (PtTPBP, Frontier Scientific) and 9, 10-bis(phenylethynyl)anthracene (BPEA, 97 %, Sigma-Aldrich) were used as sensitizer and emitter, respectively. As dispersive solvents, chloroform (99.9 %, Sigma-Aldrich) and dimethylformamide (DMF, anhydrous, 99.8 %, Sigma-Aldrich) were used. Ethoxylated trimethylolpropane triacrylate (ETPTA, SR454, Sartomer) was used as a UV curable resin. 2-Hydroxy-4'-(2-hydroxyethoxy)-2-methylpropiophenone (Irgacure2959, 98 %, Sigma-Aldrich) and 2-hydroxy-2-methylpropiophenone (Darocur1173, 97 %, Sigma-Aldrich) were used as photoinitiators for water-phase and oil-phase polymerizations, respectively. For the microfluidic emulsion system, poly(ethylene oxide)-b-poly(propylene oxide)-b-poly(ethylene oxide) tri-block copolymer (Pluronic F-108: : $(PEO)_{129}$-$(PPO)_{43}$-$(PEO)_{129}$, BASF) was used as a stabilizer in the aqueous phase. As a standard quantum counter, methylene blue hydrate (MB, ≥ 97 %, Sigma-Aldrich) was dissolved in ethanol (≥ 99.5 %, absolute, Sigma-Aldrich).

In addition, tetraethyl orthosilicate (TEOS, 99.999 %, Sigma-Aldrich), L-arginine (≥ 98 %, Sigma-Aldrich), cyclohexane (99.5 %, Sigma-Aldrich), ammonium hydroxide solution (28.0~30.0 %, Sigma-Aldrich), and ethanol (≥ 99.5 %, absolute, Sigma-Aldrich) were used for synthesis of monodisperse silica nanoparticles.

2.2. Preparation of the photocurable solution for photon upconverting capsules

For preparation of the chromophore-dispersed photocurable resin as an oil phase, PtTPBP and BPEA were initially dissolved in chloroform for dispersion and blended into ETPTA with weak sonication (2510, Branson). Insoluble impurities were removed by filtration through a 0.2 μm syringe membrane (VWR). Chloroform was selectively removed using a rotary vacuum evaporator (R-210, Buchi) at 40 ˚C, 12 mbar and then the resultant material was placed a vacuum oven at 70 ˚C for 6 hours, and the resultant prepolymer solution was purged with nitrogen for 30 minutes and degassed using a vacuum pump. The final concentration of PtTPBP and BPEA was 0.44 mM and 5.82 mM, respectively. The mixture was stored in an amber bottle at room temperature. By virtue of the observed long-term ambient stability, indeed, a glove box was not used for the anoxic process. BPEA might crystallize if it is present in too high a concentration, but this did not influence the photonic measurements. In the case of single oil-phase polymerization, 1 wt% photoinitiator (Darocur1173) was added to the mixture above.

2.3. T-junction microfluidic emulsion system

In order to produce monodisperse emulsion droplets, a T-junction microfluidic channel (PEEK Tee, IDEX) was assembled using a metal needle (33G, Hamilton Company) and capillary glass tube (Microcaps, Drummond Scientific Company) as shown in Figure 2.1. Oil and water phases were pumped (KDS100, KD Scienctific) into the inner and outer capillary at specified volumetric flow rates, where the outer diameter of the inner needle and outer capillary were 210 μm and 860 μm, respectively. The prepolymer was injected into the water containing 0.76 wt% photoinitiator (Irgacure2959) and 1 wt% surfactant (Pluronic F-108). The ETPTA emulsion droplets were stabilized with surfactant and polymerized by subsequent UV exposure using a 365 nm 4 W lamp (UVP). While the emulsion droplets exhibited a transparent complementary color against the optical bandgaps of the chromophore mixture, during polymerization PL from the

UV-excited singlet states of the chromophores was observed from the entire volume of the droplets. Stable capsules were obtained by gently rinsing several times with deionized water to remove photoinitiator and surfactant. After drying to remove residual water, a hexagonal close-packed monolayer of capsules was obtained.

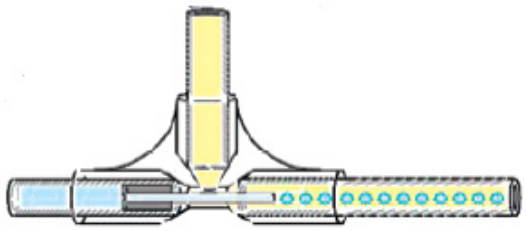

Figure 2.1. T-junction microfluidic channel assembled with capillary needle and tubes for monodisperse emulsion droplet.

2.4. Synthesis of monodisperse silica nanoparticles and preparation of photonic crystal films

As a first step to fabricate a photonic crystalline film with face-centered cubic silica arrays, monodisperse silica particles of various sizes were synthesized through sol-gel chemistry using the Stöber-Fink-Bohn method and seeded growth. In an initial stage of seed formation, TEOS was hydrolyzed in an aqueous solution catalyzed by L-arginine and delivered heterogeneously using a top layer of cyclohexane. The smallest silica seeds were preformed in a 20 ml vial and involved addition of 9.1 mg of L-arginine to 6.9 ml of water. Then 0.45 ml of cyclohexane was added to the solution and the reaction was heated to 60 °C in an oil bath. Once the temperature of solution reached the set point, 0.55 ml of TEOS was added to the vial and the reaction then kept at a constant stirring rate and temperature for 20 hours. The optional regrowth temperature remains at 60 °C since it allows use of lower arginine concentrations and minimizes secondary seed creation. To regrow the silica seeds, an appropriate portion of the seeds was taken and L-arginine, cyclohexane, and TEOS were added using the same method as previously

described. The reaction was allowed to proceed for 30 hours while maintaining a constant stirring rate and temperature. Repeating the experimental procedure one more time, the third seeds were obtained and used as intermediate seeds for further regrowth using the Stöber process. In the seed preparation step, TEOS was introduced as a silica precursor, and cyclohexane is for releasing the precursor slowly into the aqueous layer and preserving TEOS prior to its partitioning into the reaction. And L-arginine has been used as a base catalyst of silica hydrolysis and for silica particle stabilization. In a further regrowth reaction, the third silica seeds were dispersed into an ethanol solution containing water and ammonia with the total concentration in the final mixture being 11 and 1.2 M, respectively. Upon uniform mixing, TEOS was added over several hours in dropping mode by using a syringe pump. Thus, larger monodisperse silica nanoparticles of a desired size can be conveniently prepared through tuning the regrowth conditions.

The silica particles were washed several times with ethanol before use for photonic crystal films. The silica particles were redispersed into ethanol and mixed with ETPTA containing Darocur1173 at various volume fractions. After selective evaporation of ethanol from the mixture using a rotary vacuum evaporator at 40 ˚C, 12 mbar, a silica-ETPTA prepolymer solution was obtained. To fabricate colloidal crystal films, a slide glass and cover glass with a 50 μm thick polyimide tape (Kapton) as the spacer were used. The capillary-induced infiltration of the silica-in-ETPTA suspension was photo-polymerized using 365 nm 4 W UV irradiation (UVP) for 10 sec.

2.5. Measurements and characterizations

The photoluminescence (PL) properties of the individual capsules were inspected using a confocal microscope (LSM 510 Vis, Zeiss) equipped with 633 nm laser for excitation, and 650 nm long-pass and 465-510 nm band-pass filters for detection. The cross-sectional image of the core-shell structure was observed using field emission-scanning electron microscopy (Untra60 FE-SEM, Zeiss) after cutting by a blade and

washing with ethanol. The samples for SEM were coated with platinum to render them conductive. Absorption measurements were carried out using a 1 cm by 1 cm quartz cuvette via a UV-Vis spectrometer (8453, Agilent). For PL measurements, 620±1.5 nm light was used as an excitation source through a spectrofluorophotometer (RF-5301pc, Shimadzu). Also, observation of fluorescence was performed using an optical microscope (TE2000-U with Intensilight, Nikon). The elastic properties were observed using a digital microscope (VHX-60, Keyence) and measured with a nano-indenter (TI 900, Hysitron). All of the measurements were performed at room temperature and none of the investigated samples showed any photo-degradation during measurement.

Transmission electron microscopy (TEM) images for silica nanoparticles were taken with a Hitachi HF-2000 electron microscope operated at 200 kV. Sample particles were placed on a carbon/formvar film supported by a copper grid (Ted Pella, Inc.). The structure and reflectance spectra of the photonic crystal polymer were observed using SEM after platinum coating, and by an optical microscope (Leica DM4000 M) with a point-shot spectrometer (Craig), respectively. Upconverted photoluminescence intensities of PtTPBP/BPEA-dispersed ETPTA polymer films with a photonic crystal structure were measured using a fluorimeter (Spex Fluorolog-2 spectrofluorimeter) in the front face mode. All spectra have been corrected by subtraction of the spectrum of a blank sample and by introduction of the instrument correction factor, which accounts for the wavelength dependence of the instrument response function as well as for variations in excitation lamp power.

CHAPTER 3

RESULTS AND DISCUSSION

3.1. Interfacial polymerization via microfluidic system

The overall efficiencies of TTA-assisted upconversion are determined by the diffusion length of the triplet excitons; spatial overlap between the donor and acceptor wave functions is required for exchange interaction via TTET and TTA.[16,35-37] To maximize energy migration in multicomponent UC systems, molecular diffusivity of the chromophores within an inert medium is of paramount importance, especially in a solid-state matrix, for practical operation. Therefore, many rubbery low glass transition temperature polymers have been investigated.[5,16,38-40] However, even within such matrices, molecular mobility is restricted in comparison to that of identical molecules in organic solvents resulting in much lower fluorescence efficiencies in the solid system. Dye-doped polymer nanoparticles have been studied as an alternative,[41] but stable upconverted emission is yet to be demonstrated under ambient conditions.

As an alternative method, a microfluidic approach was employed for developing an air-stable dual phase UC system composed of uniform capsules fabricated by utilizing a photocurable resin. The capsules comprise a core-shell structure consisting of a fluidic active core which allows for high translational mobility of the chromophores thus preventing the large decrease in efficiency observed in solids, and an elastomeric shell for mechanical integrity to allow facile integration into a device. Through controlled photopolymerization at the surface of a microdroplet, diffusive energy transfer-driven photoluminescence in a bi-molecular UC system was explored with concomitant tuning of the properties of the capsules.

Microfluidics provides for microemulsions with desirable properties such as good sphericity and narrow size distribution.[42] As shown in Figure 3.1, the coaxial-flow microfluidic device composed of a T-junction system effects shear-induced emulsification of the chromophore-dispersed prepolymer solution. The solution was injected through the inner needle, while an aqueous phase containing photoinitiator and surfactant was introduced through the outer glass tube. At the end of the needle, the continuous outer stream served to elongate the oil flow, eventually affording a stream of highly monodisperse spherical droplets. Upon UV irradiation, free radicals are produced in the aqueous phase based photoinitiator which diffuse into the oil phase. Polymerization then occurs at the inner surface of the emulsion. The degree of polymerization is easily controlled through the UV curing time, providing the ability to finely tune shell thickness and flexible robustness.

For a given device geometry, the size and production period of the emulsion droplets is determined by the flow rate. Droplets were generated whenever the drag force was counterbalanced with the capillary force in the dripping regime.[43] Increasing the flow rate of the continuous phase resulted in a decrease in droplet size. With an increase in flow rate of the dispersion phase, the droplet size enlarged, but it was rapidly saturated followed by a gradual decrease in production interval. Figure 3.2 shows fluorescence optical microscope images of monodisperse emulsions with several droplet sizes produced by a change in flow rate; and the relationship of droplet size as a function of the continuous and dispersion phase flow rates.

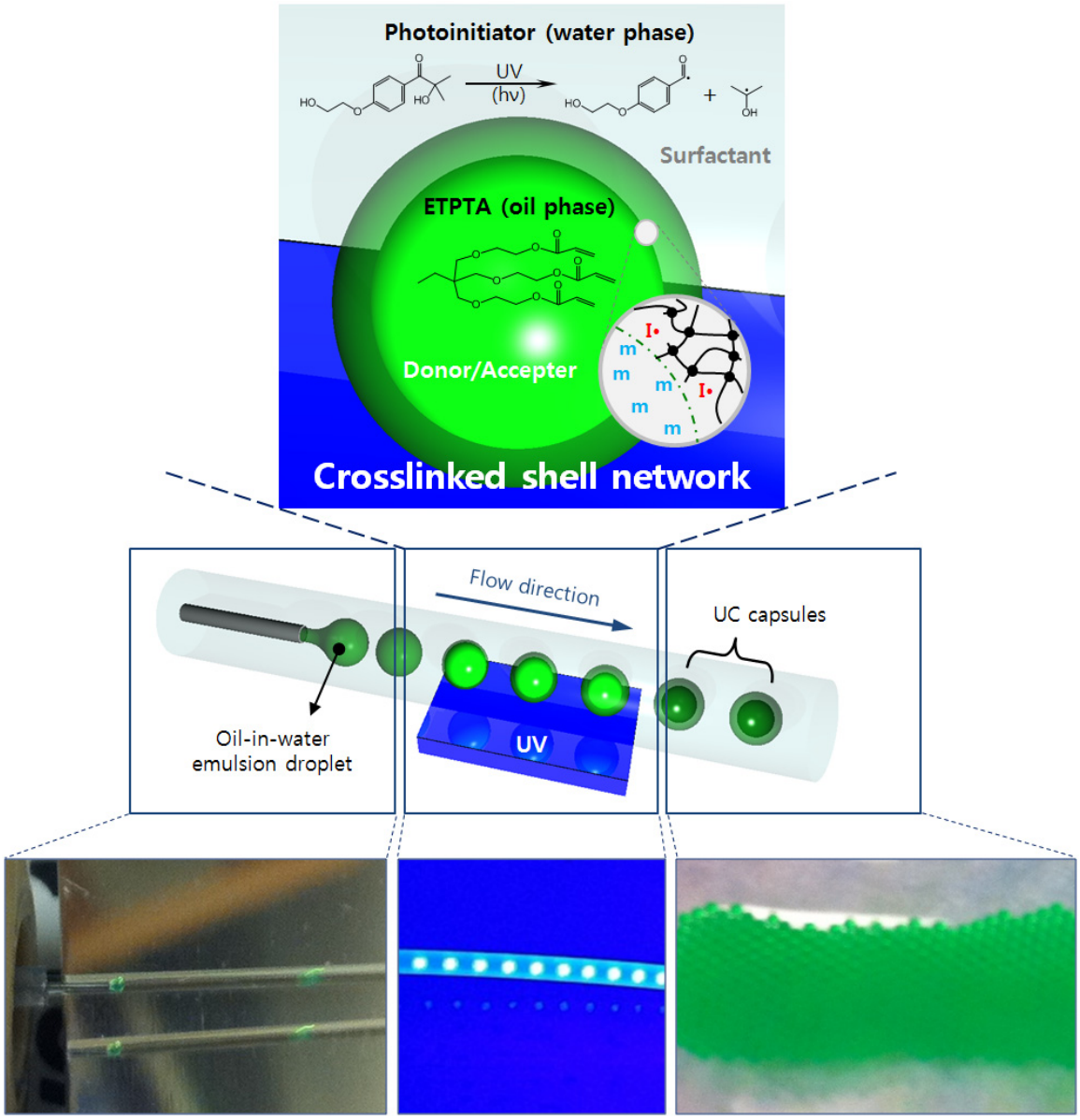

Figure 3.1. Fabrication of monodisperse photon upconversion capsules via interfacial free radical photopolymerization.

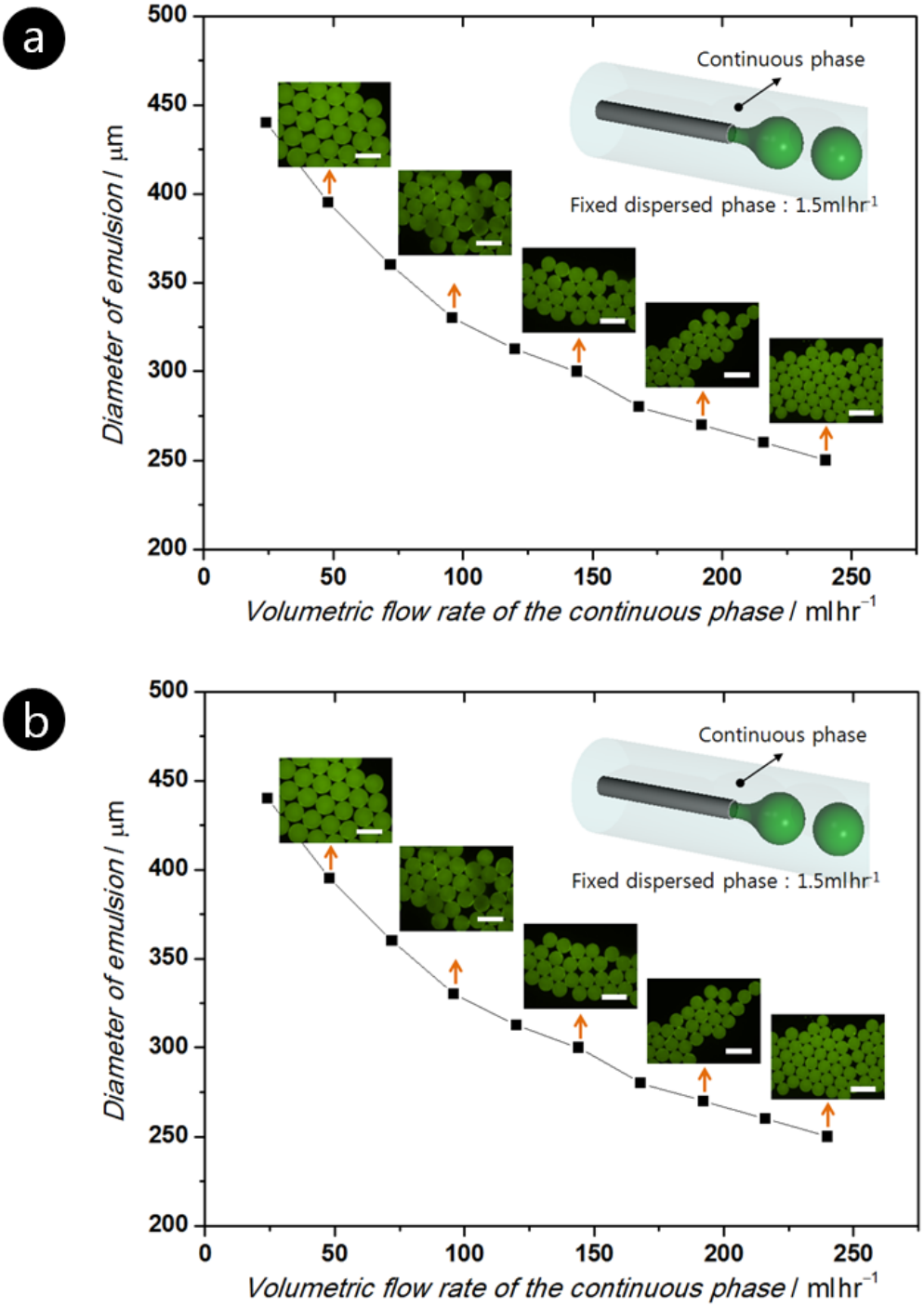

Figure 3.2. Size control of the emulsion droplets using the volumetric flow rate of (a) the continuous phase and (b) the dispersion phase. Insets are green-filtered fluorescent optical microscope images taken under blue light. All scale bars are 500 μm.

3.2. Bi-molecular TTA-based photon energy upconversion

To demonstrate the concept, platinum(II)-tetraphenyltetrabenzoporphyrin (PtTPBP) and 9,10-bis(phenylethynyl)anthracene (BPEA) were used as the donor and acceptor, respectively. Figure 3.3 presents the normalized absorbance/PL spectra and corresponding energy level diagram for a pair of PtTPBP and BPEA dispersed in ethoxylated trimethylolpropane triacrylate (ETPTA) monomer solution. ETPTA was selected as the processable medium for the UC capsules because[44-46] *i*) it is readily polymerized with UV light to afford a moldable transparent resin, and *ii*) many alternative chromophores can be well-dispersed at high concentrations due to the high polarity, low viscosity and non-volatility of ETPTA.

With respect to the chromophores, PtTPBP exhibits Soret- and Q-bands at 430 nm and 620 nm, respectively. Upon selective excitation of the latter, intersystem crossing (ISC) allows for generation of the triplet excited state of the donor. Although this triplet can revert to the ground state via phosphorescence at 770 nm without energy transfer, it is sufficiently long-lived such that it may diffuse to be in close proximity to the acceptor allowing for triplet-triplet energy transfer (TTET), leading to formation of the triplet excited state of BPEA. Finally TTA can convert two triplet states to one singlet excited state of the acceptor that can then emit higher energy photons (2.43 eV, 510 nm) than those of the incident light (2 eV, 620 nm).

According to Dexter energy transfer (by the Perrin approximation at the diffusion limit, $k_{ET} = 4\pi DC_A R_0$, where D is the overall diffusion coefficient, C_A is the acceptor concentration, and R_0 is the characteristic interaction distance),[37,47] the fluorescence derived via TTET and TTA is significantly affected by molecular diffusivity within a given medium. The quantum yield of the upconverted fluorescence for the PtTPBP-BPEA system as a function of BPEA concentration is shown in Figure 3.4. At a fixed

PtTPBP concentration (~1.01 μM), quantum yield was saturated with increasing BPEA concentration. Although the more viscous ETPTA liquid solution (60 cP) vs. dimethylformamide (DMF, 0.92 cP) initially exhibits relatively lower quantum efficiency due to reduced diffusive interactions, ETPTA retards the penetration of oxygen which rapidly quenches the excitons. Notably, efficiency in bulk ETPTA remains almost constant even after 5 days in air. Further, within a freestanding film, UC efficiency using a UV-cured ETPTA control matrix is higher than that observed from a commercial rubbery polyurethane film. Thus, the ETPTA encapsulation method described here can facilitate vital collisional energy transfer, especially within a liquid phase core providing for highly efficient UC emission with enhanced stability.

The relative quantum efficiencies for upconverted fluorescence were measured as a function of BPEA concentration, relative to methylene blue in ethanol as the standard ($\Phi = 0.04$).[48] Calculations were carried out using Equation (1), where, Φ_{UC}, A_{UC}, I_{UC} and n_{UC} represent the quantum yield, absorbance, integrated photoluminescence intensity, and refractive index of the medium of the upconversion system. The corresponding terms for the subscript 'std' are for the standard counter at the indentical excitation wavelength. The factor of 2 is included since the TTA-assisted upconversion process requires the absorption of two photons to convert one photon whereas the standard counter emission is directly proportional to the incident number of photons.

$$\Phi_{UC} = 2\Phi_{std}\left(\frac{A_{std}}{A_{UC}}\right)\left(\frac{I_{UC}}{A_{std}}\right)\left(\frac{n_{UC}}{n_{std}}\right)^2 \quad (1)$$

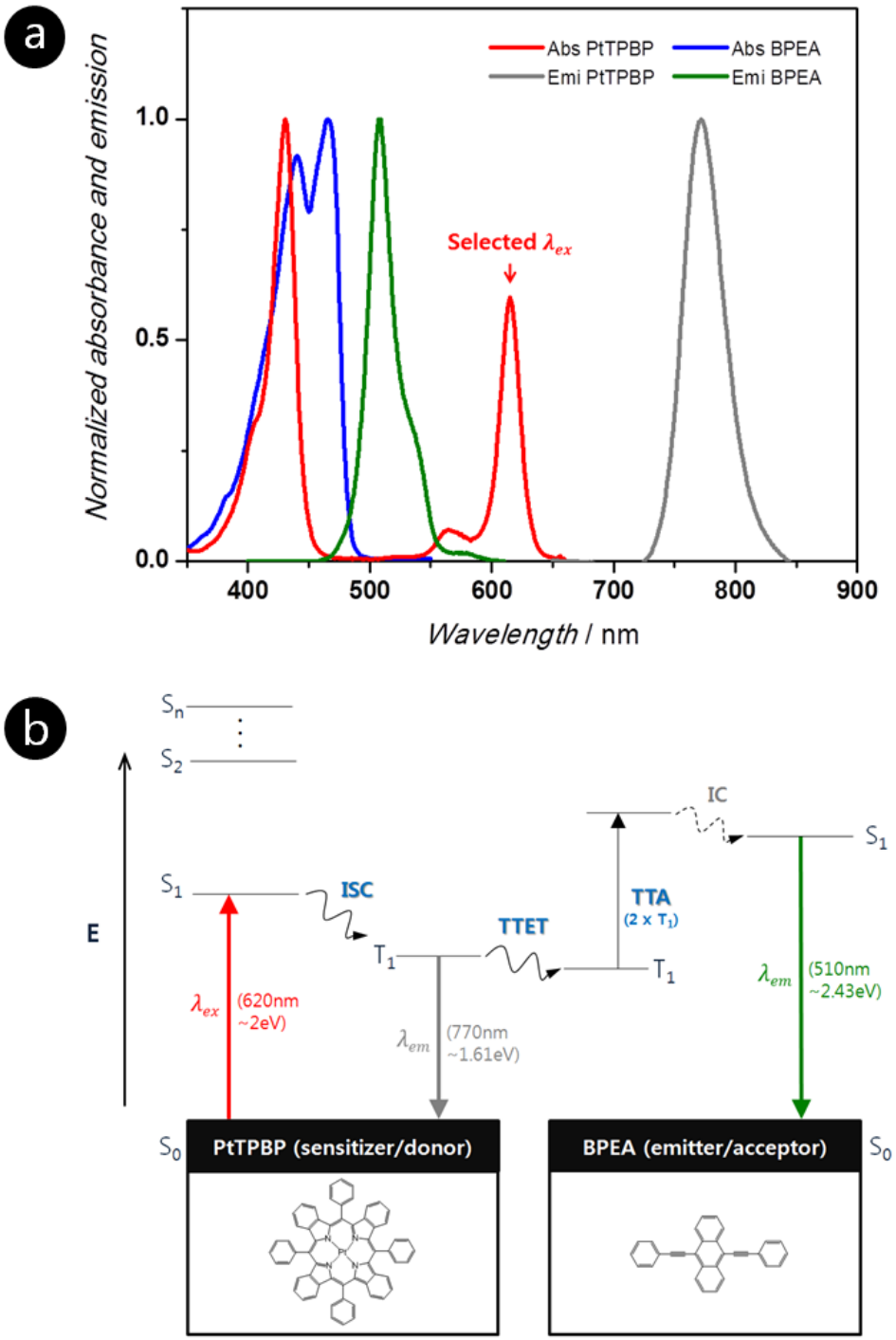

Figure 3.3. (a) Normalized absorbance and photoluminescence spectra of PtTPBP and BPEA dispersed in ETPTA monomer solution. The selected excitation wavelength of the sensitizer was used for this study. (b) Energy level diagram of TTA-assisted UC process and molecular structures of PtTPBP and BPEA.. The colored solid arrows indicate possible radiative absorption (red) and emission (grey and green), corresponding with (a).

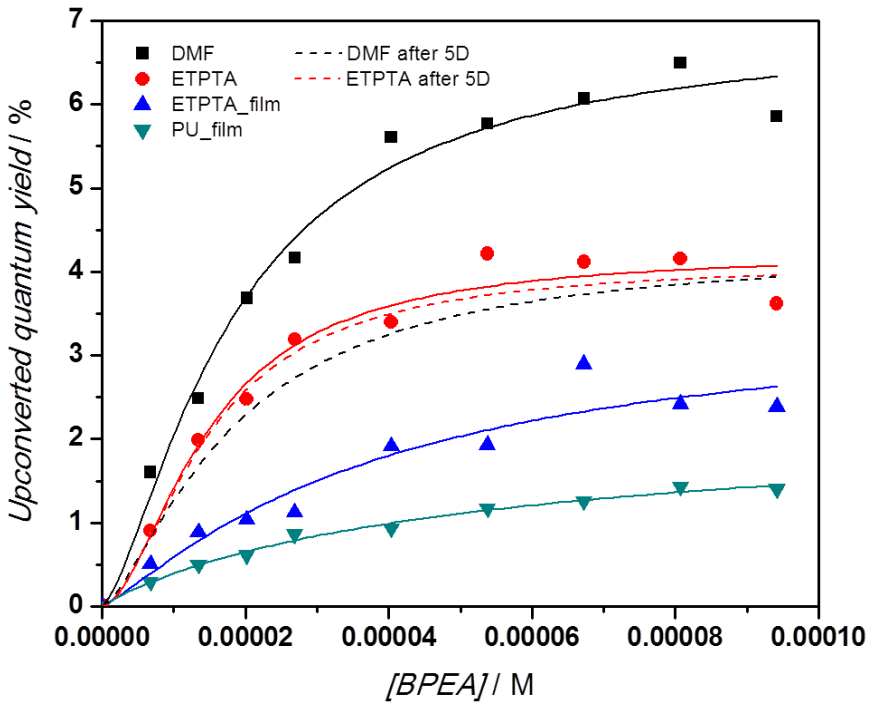

Figure 3.4. Relative upconverted fluorescence quantum yield within different media as a function of BPEA concentration under selective excitation of PtTPBP (33.5 μW 633±1.5 nm).

3.3. Microscopic characterization of UC capsules

The relationship between the focal plane and PL intensity shown in Figure 3.5 indicates how the plane was focused on the circumference of the capsule at the equator. The confocal microscope images show cross-sectional views of the same capsule at four different focal planes, ranging from the z-plane at 17 μm to at 221 μm. The insets from the transmitted bright field mode indicate the degree of focus on the capsule. In addition, the corresponding profiles indicate relative intensities of upconverted and downconverted emission, definitely confirming the core-shell structure of the capsule. In the centered magenta signal at the 17 μm z-plane, phosphorescence of the sensitizer was mainly observed in the highly crosslinked shell, which has only a small probability of collisional energy transfer due to the short diffusion length of the excitons in this medium. The next 85 μm z-plane shows the highest intensity of both TTA-based fluorescence and

phosphorescence relative to the other z-planes examined here, which implies maximum absorption and energy transfer occurred up until this limited plane. This is the reason that the central intensity at the 153 μm z-plane is lower than at 85 μm, although it is clear-cut focused. However, its onset points and peaks of PL admittedly define the interface between the core and shell. Out of focus at 221 μm, both intensities diminished remaining faint at the interfacial boundary.

The capsule shell thickness can be controlled via UV exposure time. Here, the range from 33 to 120 seconds under 3.7 $mWcm^{-2}$ 365 nm illumination was used, and the impact of shell thickness on capsule PL was investigated. Figure 3.6 depicts confocal microscope images at the clear-cut focal plane of the capsules. Two distinctly different emission bands were observed, one associated with the core and another from the shell. The intensities of these bands are dependent upon the respective diffusivities of the chromophores and required molecular energy transfer; upon 633 nm excitation, annihilation fluorescence induced green emission emanates from the core , whereas the magenta signal derives from emission associated with phosphorescence of the sensitizer through the crosslinked shell (confocal microscopy shows merged monochromic pseudo-colors). Increasing UV curing time leads to a thicker downconverted PL region, which indirectly indicates shell thickness. However, these results do not imply that the crosslinked shell is unable to produce detectable upconverted emission. Because TTA-assisted UC is a nonlinear process, the shell was also observed to release delayed fluorescence when stimulated with a high power excitation source. The corresponding profiles display the relative intensities of upconverted and downconverted emission. Their onset positions coupled with the PL peaks define the interfaces between the core and shell of the capsules, confirmed by both the transmitted images displayed in the insets and scanning electron microscope images shown in Figure 3.7. If the shell layer was too thin, the capsules did not have sufficient mechanical strength and the core resin easily leaked out upon washing and drying. An overly thick shell layer reduces the

volume of the core leading to a reduction in upconverted emission. With controlled UV exposure, the solid capsule shell has reversible elastic properties and no leakage of core contents was detected (Figure 3.8).

Since each capsule behaves as a single, isolated photon upconverting unit, it can be used as a building block for a multi-dimensional optical system. Uniformly sized capsules enable self-assembly of the structures into a hexagonal close-packed monolayer array and the relative PL yield is determined by the number of capsules per unit area. As illustrated in Figure 3.9 (a), bluish green emission from the array was generated at the region of excitation in Figure 3.9 (b). Although a portion of red excitation light was scattered at the surface of the capsules due to their spherical shape and refractive index difference between air and ETPTA (n~1.469), a bandpass filter allowed for distinguishing upconverted emission from scattered light of the source. Fluorescence optical microscopic images also depict the dramatic emissive response of the capsules. While upconverted emission is barely discernible under conditions of no excitation (top) or filtered blue light (middle), the bottom image shows the intensively condensed emission from the capsule cores upon excitation with a conventional laser pointer. Figure 3.9 (c) depicts the relevant PL intensities of monodisperse capsule arrays with different shell thicknesses (as described in Figure 3.1). Integrated spectra of upconversion at a 510 nm peak and downconversion at 770 nm were obtained under exposure to 0.165 $mWcm^{-2}$ 620±1.5 nm radiation. As UV curing time increases, upconverted peaks diminish while downconverted bands ascend dramatically. This phenomenon can be explained by both the formation of one excited singlet state obtained from two sensitizer triplet states via sequential energy transfer, and a large volume change of the shell.

Meanwhile, the shield offered by encapsulation prolongs the natural lifetime of the process by retarding oxygen penetration which typically quenches the excited states in organic systems and represents a significant drawback for standard TTA-assisted upconversion processes.[14] For evaluation of capsule stability, integrated upconverted PL

was measured as a function of time in ambient air, as shown in Figure 3.9 (d). Except for the first two samples receiving the shortest UV curing times (33 and 40 seconds), most of the core-shell structured capsules appear very stable, with no apparent reduction in PL intensity over 240 hours. Thus, through appropriate control of shell thickness, the active core is readily protected from the ambient.

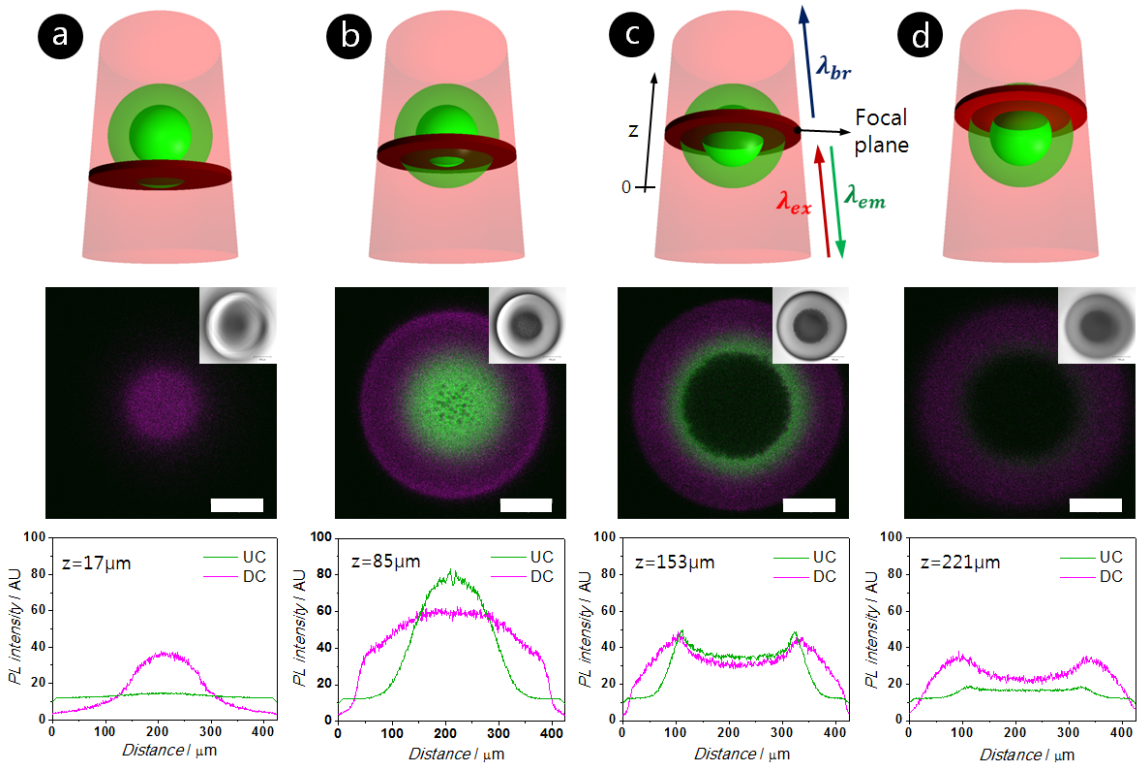

Figure 3.5. Confocal microscope images and the corresponding photoluminescence profiles of the capsule at different focal planes. Each inset shows the monochromic transmitted bright field image. All scale bars are 100 μm.

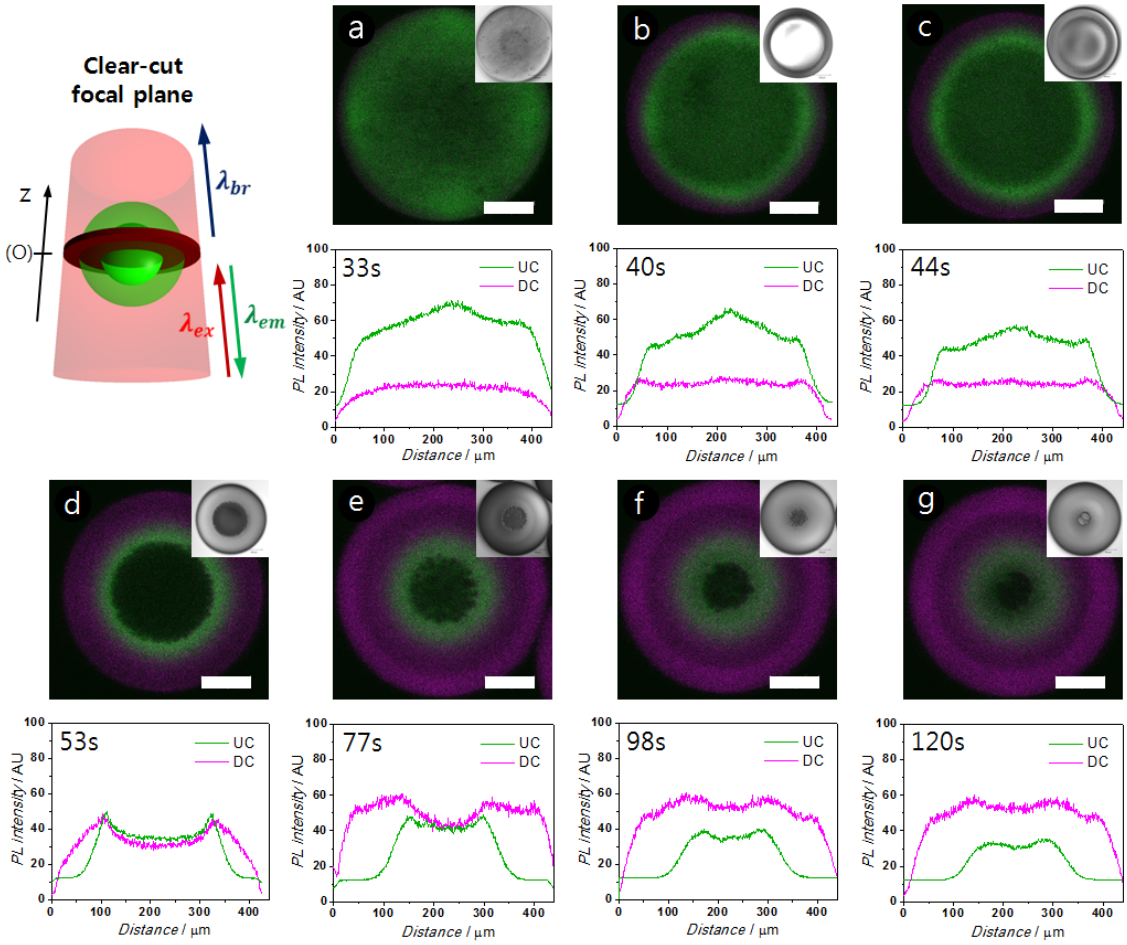

Figure 3.6. Confocal microscope images and the corresponding upconverted (UC) and downconverted (DC) photoluminescene profiles at clear-cut focal plane of capsules with variable UV curing times. Each inset shows monochromic transmitted bright field image. All scale bars are 100 μm.

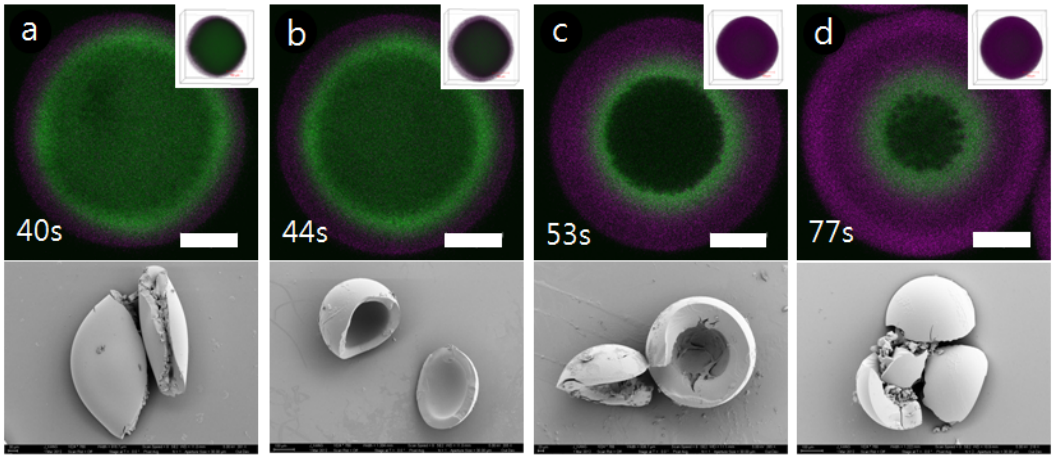

Figure 3.7. Confocal microscope images at the clear-cut focal plane shown in Figure 3.6 (b)-(e) and the corresponding scanning electron microscope images after blade-cutting and washing with ethanol. Each inset shows three-dimensional photoluminescence on the surface. All scale bars are 100 μm.

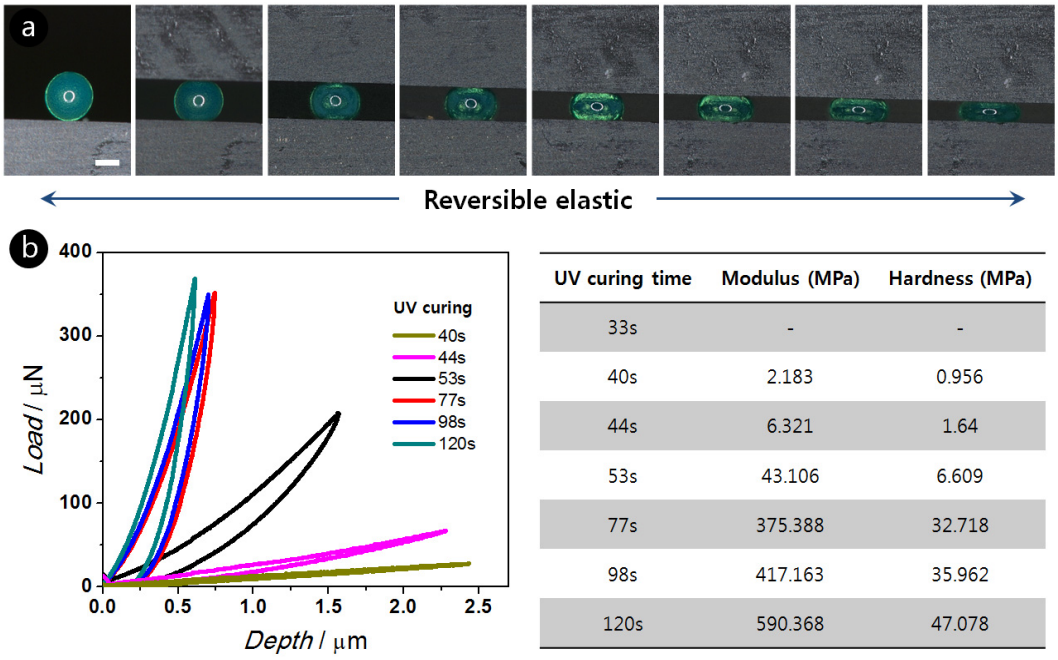

UV curing time	Modulus (MPa)	Hardness (MPa)
33s	-	-
40s	2.183	0.956
44s	6.321	1.64
53s	43.106	6.609
77s	375.388	32.718
98s	417.163	35.962
120s	590.368	47.078

Figure 3.8. Digital microscopic images of capsules pressed between two slide glass plates. The scale bar is 200 μm. (b) Modulus and hardness of the capsule shells with respect to UV curing time.

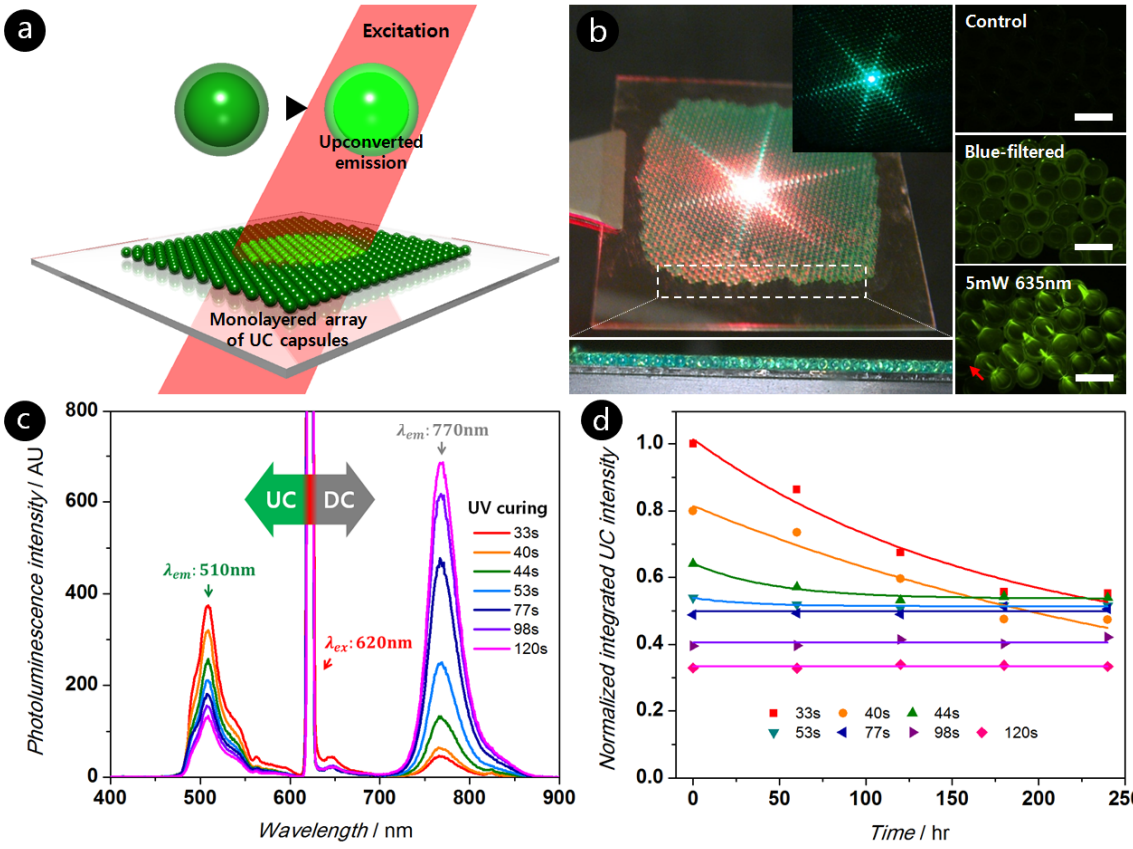

Figure 3.9. (a) Schematic illustration of upconverted emission from monolayered array of capsules, (b) Digital image of photoluminescence of the array under a focusable 5 mW 633 nm laser (inset shows 520 nm bandpass (FWHM = 10±2 nm)-filtered emission) and optical microscopic images; (top) without excitation for control, (middle) under the blue filtered light, and (bottom) excited by a 5 mW 635 nm laser pointer. (The red arrow indicates the direction of the lasing light). All scale bars are 500 μm. (c) Photoluminescence spectra of monolayered arrays with variable UV curing times at room temperature. The intense peak at 620 nm comes from the scattered reflection of the excitation light. (d) Normalized integrated upconverted emission intensities of the arrays shown in (c) as a function of time in ambient condition.

3.4. Enhanced photon upconversion via photonic crystal structures

To enhance photon upconverted emission, photonic crystals were employed for an optical constructive mirror. For fabrication of photonic bandgap structures, organic or inorganic colloidal suspensions of monodisperse particles can be used as building blocks. As a representative candidate, silica nanoparticles were synthesized because they can be organized into orderly face-centered cubic (FCC) lattice structures by self-assembly in a confined geometry. The self-ionization of hydroxyl groups on the silica surface provides negatively charged particles so that electrostatic interaction between the silica spheres enables them to form colloidal crystalline phases.[49]

For the generation of a monodisperse silica suspension, the Stöber method has been widely developed as a physical chemistry process since Werner Stöber discovered the method in 1968.[50] Tetraethyl silicate is stirred in an excess of water containing a low molar concentration of alcohol and ammonia. The reaction taking place is hydrolysis of the silyl ether to a silanol followed by condensation, which eventually produces silica nanoparticles and ultimately the gel network. As an example, Figure 3.10 shows a general mechanism of the Stöber reaction from Tetraethyl orthosilicate (TEOS), which is the most common precursor, to silicon oxide. The resulting silica particles have diameters between 50 and a few thousands of nanometers, depending on the nature of the silicate ester and alcohol, and their ratio.

Sol-gel chemistry tends to be extremely sensitive to external environments such as pH, temperature, humidity, catalyst and solvent.[51] It was very difficult to fabricate spherical silica particles with a narrow size distribution and high reproducibility through a single Stöber process. Therefore, a seeded-growth method was adopted to improve monodispersity and size control by disentangling the less controllable nucleation as a separate stage of formation of small seeds, and precisely regrowing the seeds under well-defined conditions. Figure 3.11 shows monodisperse silica spheres achieved by using the modified synthesis method reported by Yokoi et al.[52,53] and coupling with semi-

continuous regrowth.[54] In an initial stage of seed formation, highly monodisperse silica particles with a range from less than 20 to 55 nm were produced. Following seed formation, larger silica particles of a desired size with narrow size distribution could be prepared by controlling regrowth conditions in the same reaction medium. Meanwhile, the concentration of TEOS and arginine, a base catalyst for the hydrolysis, was one of the key factors for successful regrowth of the silica seeds; the arginine concentration should be reduced to minimize secondary seed formation of different sizes while the amount of TEOS increased.

The silica seeds were compatible with the Stöber process and thus can be readily further regrown without any purification, to arbitrarily larger size, while perfectly preserving their monodispersity. High monodispersity of the prepared silica spheres renders them perfectly suitable for colloidal array formation. The regrowth process was performed using the conventional Stöber method, but TEOS was added slowly to prevent secondary seed particle formation. As depicted in Figure 3.11 (c) and (f), much larger particles were produced by Stöber regrowth from seeds approximately 55 nm in size. Centrifugation-induced deposition of 150 nm diameter silica in ethanol has a green bandgap as shown in the inset of Figure 3.11 (f).

Conventional evaporation-induced colloidal crystallization uses emulsion or aerosol drops, cylindrical capillaries, and patterned microchannels as templates to mold the crystals into desired shapes. However, evaporation-induced crystallization requires impractically long times for complete consolidation and inevitably yields crystals with severe cracks. In the present work, using silica particles dispersed in ETPTA resin, various photonic structures were successfully fabricated with negligible cracking via evaporation-free colloidal self-assembly. The success of this system stems from the highly viscous nature of the ETPTA precursor, which causes the crystalline structure formed in suspension to be more robust against disturbances from external flows or Brownian diffusion. The ETPTA resin is photo-polymerizable under UV exposure,

enabling the capture of the colloidal crystalline structures without defects within a short time period. More importantly, the silica particles spontaneously organize into an ordered phase at low concentration on account of strong repulsive forces to a diminishing van der Waals attraction, because the ETPTA resin is highly polar and has a similar refractive index ($n_m \sim 1.469$) with that of silica ($n_p \sim 1.45$).

For practical applications, photonic crystal polymer films were prepared with varying volume fraction of silica particles (ϕ). As shown in Figure 3.12 (a), silica particles dispersed in ETPTA resin diffracted light and displayed iridescent colors at concentrations as low as $\phi \sim 0.1$. The main reflection wavelength λ depends on the particles diameter D and volume fraction ϕ, and can be estimated by Bragg's equation for a normal incident beam onto the (111) plane of an FCC structure when we assume that interparticle distance for all nearest neighbors is constant at a given volume fraction. Figure 3.12 (b) depicts structural difference between close-packed FCC via evaporation-induced crystallization and nonclosed-packed FCC via evaporation-free colloidal self-assembly. Figure 3.12 (c) shows the reflectance spectrum of a solidified photonic crystal film and its corresponding bluish green color from a normal incident white light at ambient room conditions. Also the film displays uniform reflection color, indicating that it is a high-quality photonic crystal without cracks.

Silica-in-ETPTA composites with other shapes can be readily fabricated using different templates. For example, photonic crystal films were created by inserting the suspension via capillary forces into the gap between two parallel plane glass plates separated at a distance of 2-5 mil spacer, shown in Figure 3.13. Based on the capillary-flow driven assembled photonic crystal film, chromophore-dispered ETPTA resin was applied for photon energy upconversion. After sequentially controlled UV curing, the bi-layer structure was created and provided the highly enhanced upconverted emission when the optical bandgap of photonic crystal bottom layer matches emission band of the

upconverting layer under the selected excitation. In comparison with a bare PtTPBP/BPEA-dispersed ETPTA polymer film (Figure 3.14 (a)), the photonic crystal structure-assisted upconverting film (Figure 3.14 (b)) had more than 5 times higher intensity of the emission peak at the photonic crystal bandgap, which was 520 nm as shown in Figure 3.12 (c).

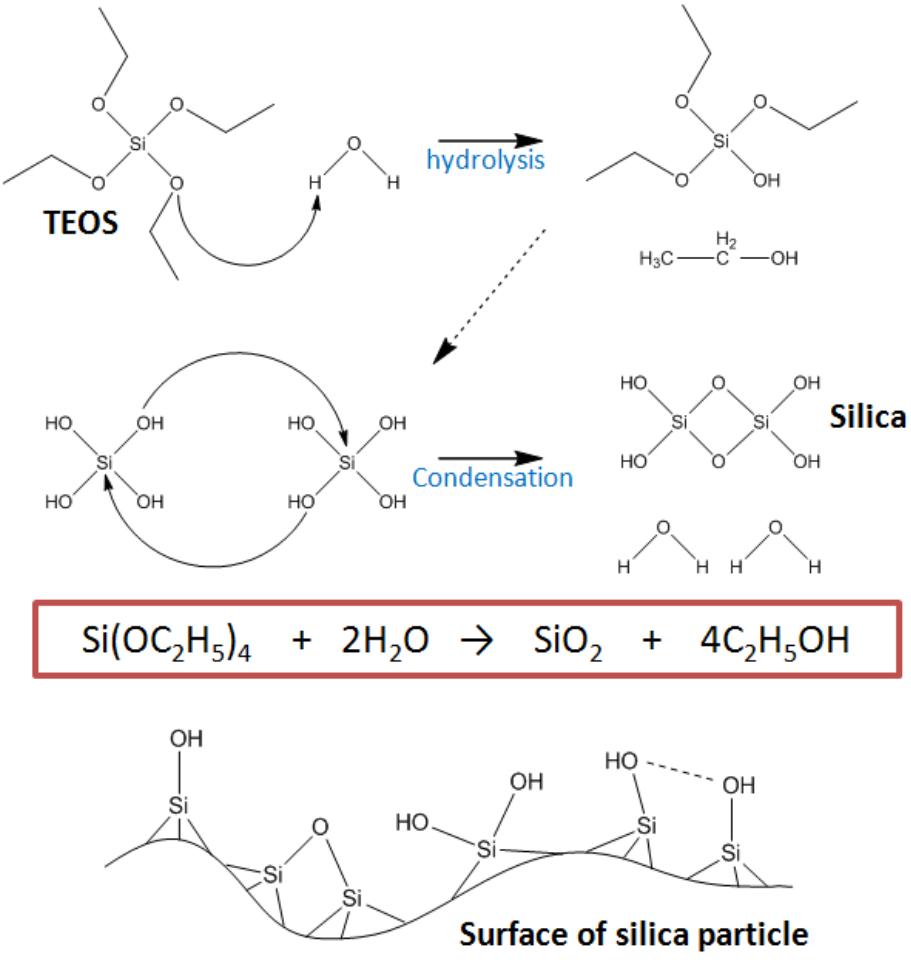

Figure 3.10. Schematic reaction mechanism of silica particle via Stöber process.

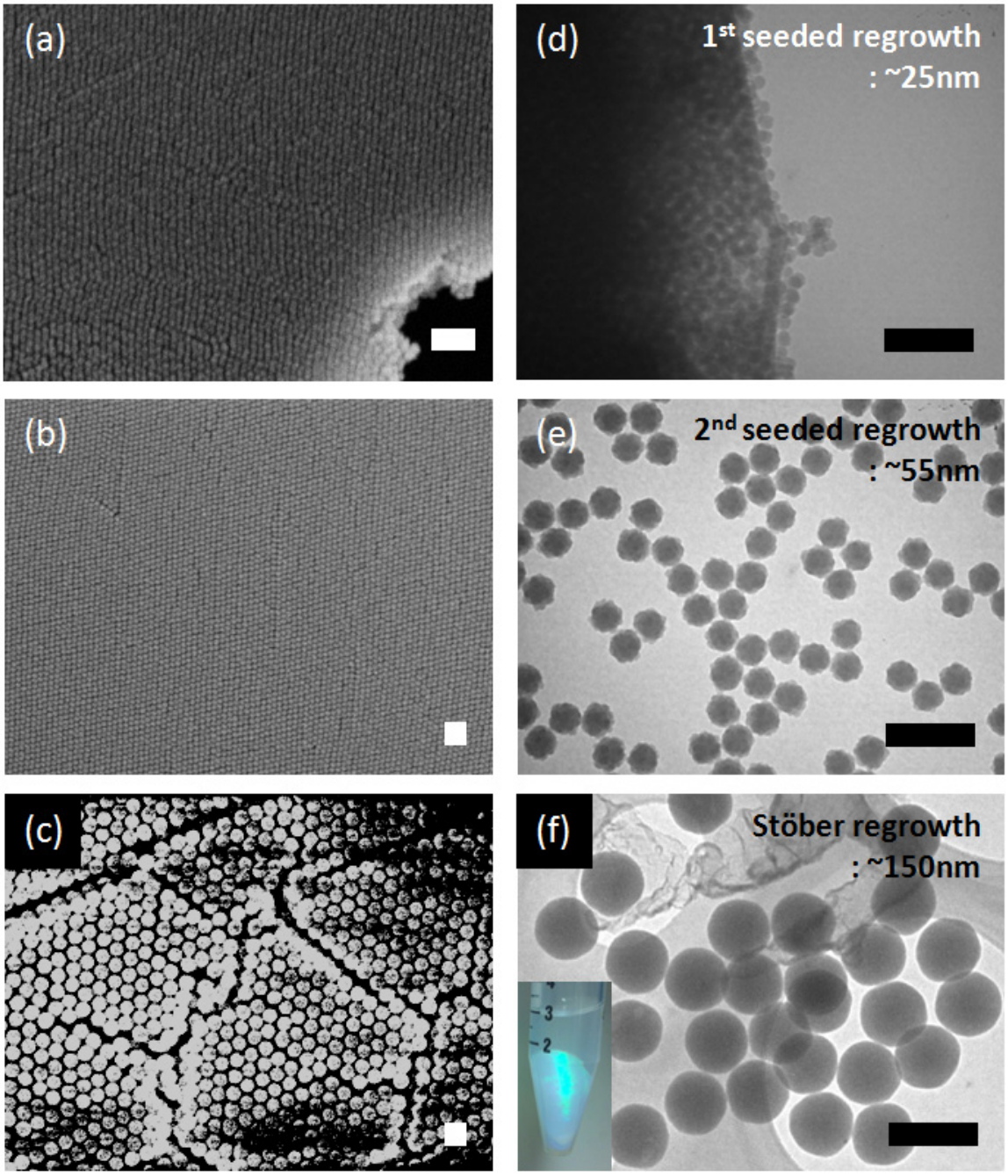

Figure 3.11. Monodisperse silica spheres achieved by two phase-based seed preparation and Stöber regrowth; (a) and (d) 25 nm silica produced first stage regrowth process from the seeds, (b) and (e) 55 nm silica seeds by second stages of regrowth, (c) and (f) 150nm silica produced by Stöber regrowth (a-c: scanning electron microscopy, d-f: transmission electron microscopy). All scale bars are 200 nm.

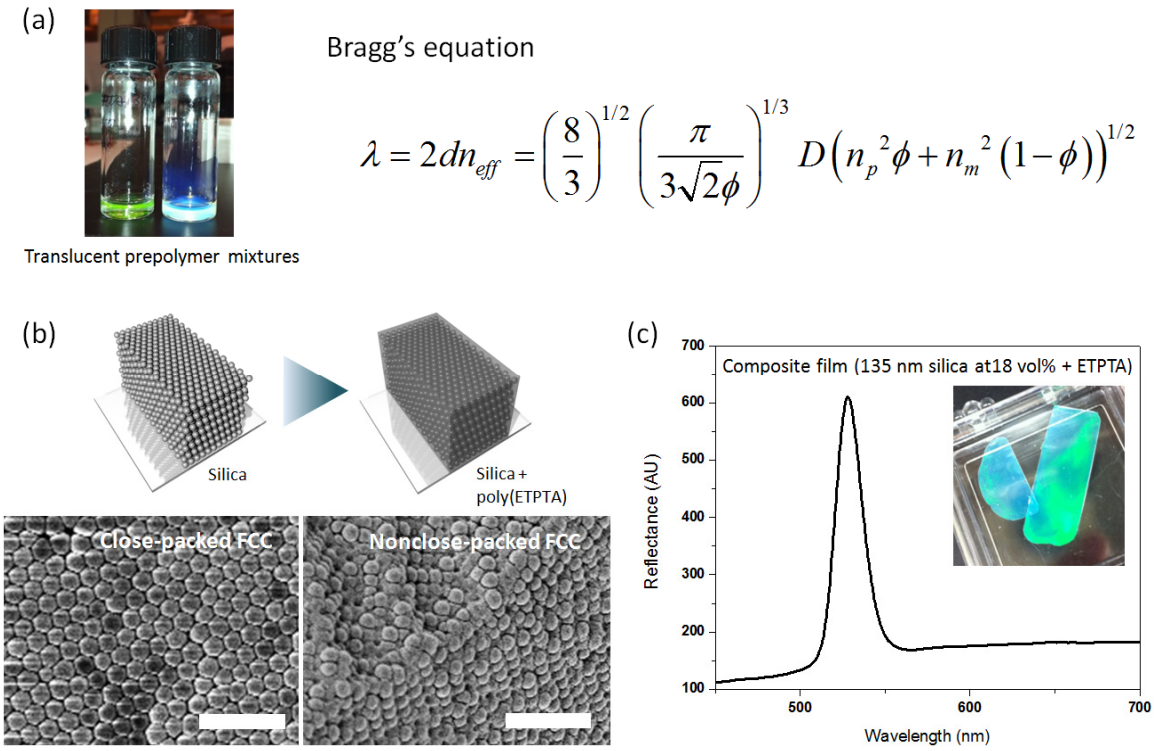

Figure 3.12. The structure of photonic crystal films and their bandgaps: (a) Iridescent colors of silica dispersed in ETPTA suspensions at different particle concentration; green and blue suspensions are composed of 135 nm silica particles at $\phi \sim 0.15$ and 0.27, respectively (The volume fraction was estimated by Bragg's equation.). (b) Structure of the photonic crystals via scanning electron microscope: left and right images show close-packed face-centered cubic (FCC) and nonclose-packed FCC, respectively. All scale bars are 1 μm. (c) Reflectance spectrum of the photonic crystal polymer film of 135 nm silica particles at $\phi \sim 0.18$ (Inset shows a bluish green color as an optical bandgap.).

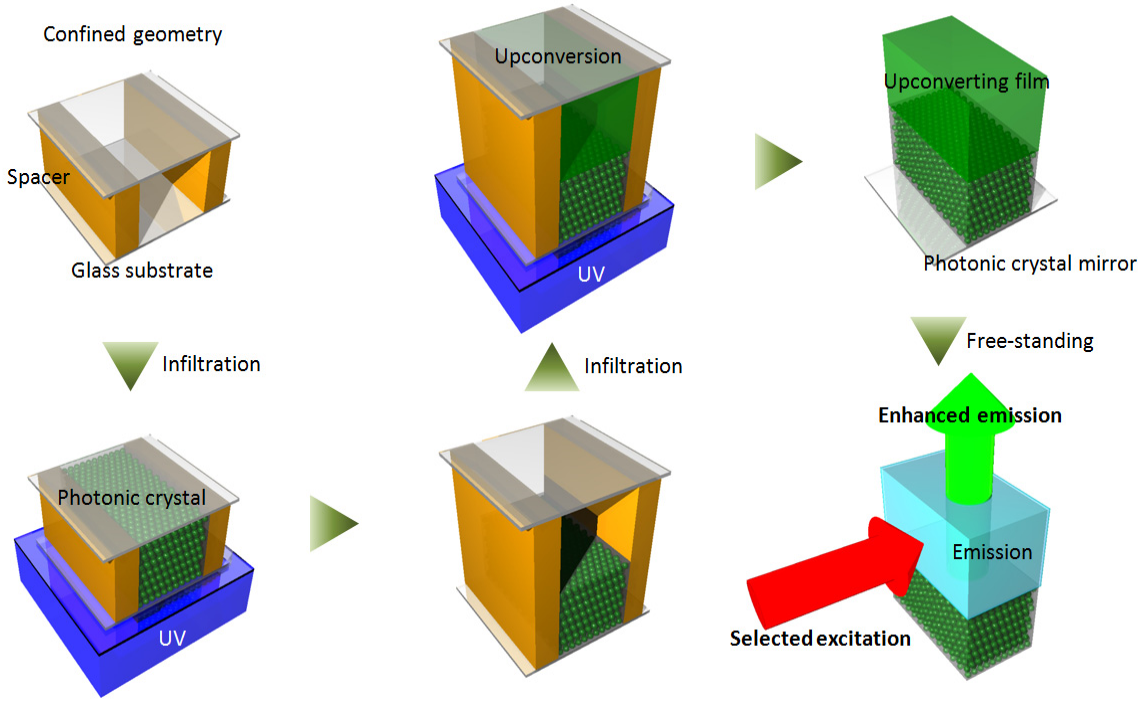

Figure 3.13. Schematic illustration of fabrication of emissive photon upconverting photonic crystal film via sequential steps of photo-polymerization.

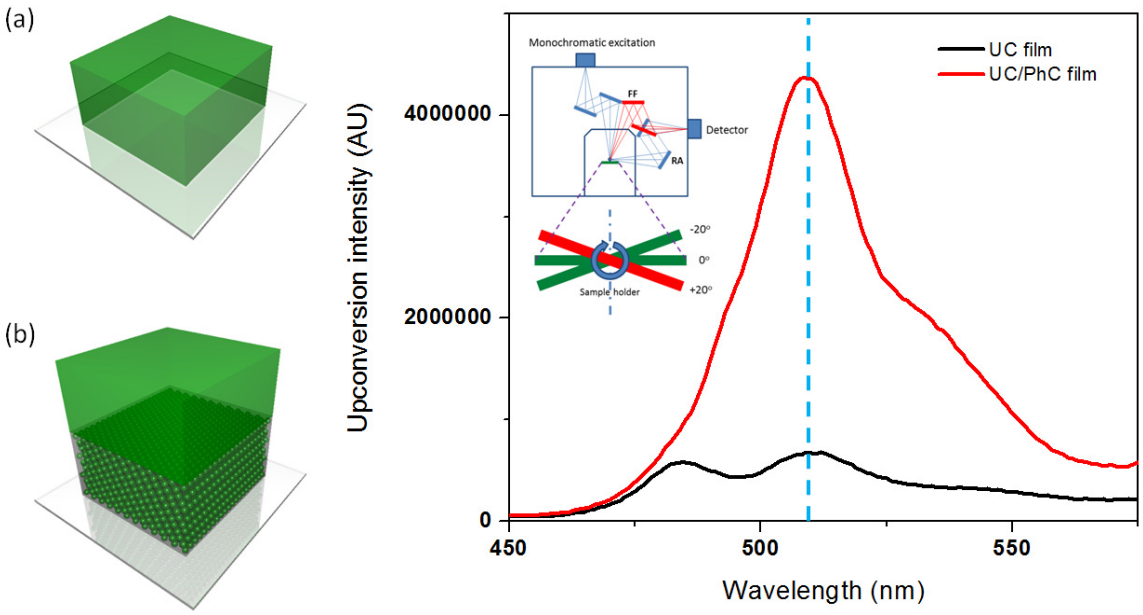

Figure 3.14. Upconverted photoluminescence intensity of PtTPBP/BPEA-dispersed ETPTA polymer films (a) without and (b) with a 520nm bandgap photonic crystal composite under 620 nm excitation (3 nm slit size) in the front face mode of fluorimeter.

3.5. Effect of energy relayed photon upconversion on dye-sensitized solar cell

Dye-sensitized solar cells (DSSCs) work on the basis of light harvesting using a sensitizing dye attached to a wide-bandgap semiconductor.[55] DSSCs are composed mainly of abundant, non-toxic materials and offer an inexpensive route to the development of highly efficient photovoltaic cells. State-of-the-art DSSCs, which absorb light from 350 from 700 nm, have validated power conversion efficiencies of over 11 %.[56] A key to improving the efficiency of DSSCs is to increase their spectral absorption range. To reach power conversion efficiencies of more than 15 %, DSSCs must absorb ~80% of the solar spectrum from 350 from 900 nm.[57] Light absorption in DSSCs is determined by the molar extinction coefficient of the sensitizing dye, the surface coverage of the dye, and the total surface area of the semiconductor film.[58] Films comprising titania nanoparticles increase the surface area so that the sensitizing dye can be covered over the large area. Traditionally, sensitizing dyes have been made from ruthenium-based complexes such as N-719 that have a fairly broad absorption spectrum but low molar extinction coefficients.[56]

Co-sensitization of titania by dyes with complimentary absorption spectra has been demonstrated to enhance light absorption and broaden the spectral response of organic DSSCs.[59] In particular, a recent study has demonstrated the use of Föster resonant energy transfer (FRET) between chromophores inside the liquid electrolyte and sensitizing dye attached on the titania surface.[60,61] The chromophores can absorb high-energy photons and efficiently transfer the energy to the anchored sensitizing dye, increasing the absorption bandwidth of the DSSCs. However, the overall power conversion efficiency of the DSSC was low (3.21 %) because they used the near-infrared sensitizing zinc phthalocyanine dye which can absorb light only over a small spectral region and the excited dye can be non-radiatively quenched by a salt such as triiodide in the chloroform as a electrolyte.

In order to utilize a broad range of the solar spectrum without quenching by an electrolyte in DSSCs, contructively enhanced light emission should be seperated from the quenchant and matched with absorption peaks of the sensitizing dye for secondary energy relay transfer. As shown in Figure 3.15 (a), a photon energy upconverting mirror including a pair of PtTPBP and BPEA was demonstrated on a typically structured DSSCs using N-719 (Figure 3.15 (b)). In particular, a photon upconversion layer allows the use of inferior solar photons without any change of the sensitizing dyes for primary absorption so that the overall power conversion efficiency of the solar cell will not be reduced. Figure 3.15 (c) describes normalized absorbance spectrum of N-719 where it has two strong peaks at about 380 and 520 nm, but a weak tail above 600 nm. Meanwhile, the red-to-green upconverting system via PtTPBP and BPEA shows a strong absorption band at 620 nm and emission band at 510 nm (Figure 3.12 (c)), which are perfectly matched with a weak and strong absorbance of N-719, respectively.

The bluish green light from the exteral upconverted layer was generated even though the number of transmitted photons through a solar cell is less. As shown in Figure 3.16, the emission enhanced the incident photon to charge carrier efficiency (IPCE) of the DSSC at about 600 nm, while the photonic crystal with a 520 nm bandgap improved IPCE at its reflectance spectrum. However, the bi-layer structure comprising an upconverting film and a photonic crystal was not a fair representation of possible increases in IPCE, because a solid state upconverting film was used. To avoid reducing the quantum efficiency of the upconversion system, a liquid state upconverting film also was investigated by measurement of power conversion efficiency of DSSCs, where dimetyhlformamide (DMF) was used as a relatively non-volatile organic solvent with high boiling point (153 °C). Under an overall solar spectrum at 1.5G, the efficiency of a DSSC was significantly increased via upconverted emission (Table 3.1). The more than 15 % increase in device performance is attributed to the increase in the short-circuit photocurrent density (J_{sc}) caused by an increase in light usage in the range of 550 to 660

nm as shown in Figure 3.16, while the fill factor and open-circuit voltage (V_{oc}) remained relatively unchanged. Furthermore, when a 400 nm longpass filtered excitation source was applied to the DSSCs rather than 590 nm, both up- and down-converted emission of the accepter molecules, BPEA, was generated at the same time so that more intense light improved the device performance by as much as 20 %.

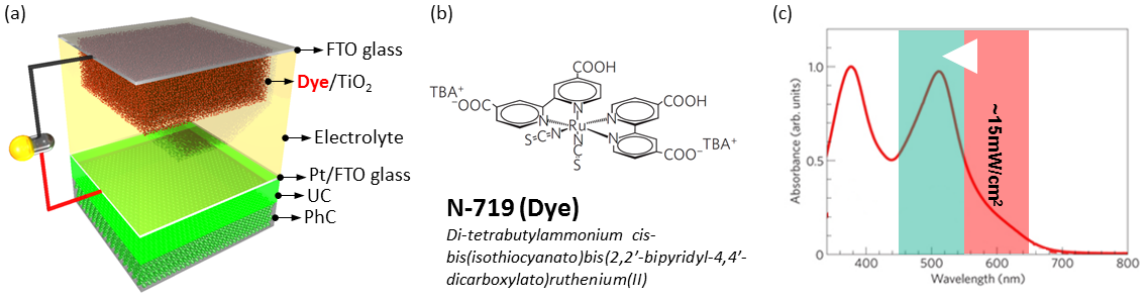

Figure 3.15. (a) Schematic structure of dye-sensitized solar cell with photon upconverting mirror layer, (b) Molecular structure of representative sensitizing dye,[62] and (c) Normalized absorbance spectrum of N-719[62] and a strategy of upconverted emission band (blue shadow) from the selected excitation (red shadow), which is corresponded with absorption of PtTPBP as a donor.

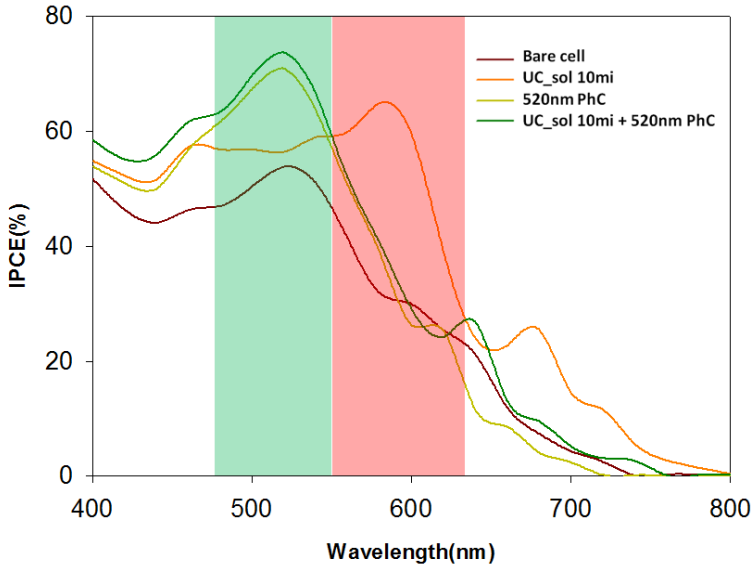

Figure 3.16. Effect of external photonic layers on incident photon to charge carrier efficiency (IPCE) of dye-sensitized solar cells using N-719 anchoring on titania nanoparticles.

Table 3.1. Photovoltaic characteristics of dye-sensitized solar cell by using liquid state upconversion film.

	Control			Upconversion (liquid state)		
Solar spectra	**DMF**	**DMF(>400)**	**DMF(>590)**	**UC**	**UC(>400)**	**UC(>590)**
Area(mm^2)	10.65	10.65	10.65	10.65	10.65	10.65
Jsc(mA/cm^2)	11.43	10.47	3.84	12.19 (6.65% ▲)	11.51 (9.93% ▲)	4.22 (9.9% ▲)
Voc(V)	0.761	0.761	0.696	0.761	0.761	0.696
FF	0.520	0.537	0.553	0.564	0.589	0.580
Efficiency (%)	4.519	4.278	1.477	5.225 (15.6% ▲)	5.152 (20.4% ▲)	1.703 (15.3% ▲)

CHAPTER 4

CONCLUSION

4.1. Low-threshold photon upconversion capsules via photo-induced interfacial polymerization

In conclusion, we have designed an effective approach to provide for low-threshold TTA-based UC within a structure that could be readily incorporated into a photonic device using conventional processing methodologies. The fabrication of monodisperse core-shell UC microcapsules using UV-initiated free radical inverse polymerization through a microfluidic channel has been demonstrated. A photocurable resin served as both a medium for TTA-based UC and a shell for practical passive protection. By taking advantage of the liquid core-solid shell structure, self-assembled capsule arrays were shown to offer outstanding optical emission under ultralow power excitation coupled with high mechnical integrity and strength. We believe that this two-phase structure has significance not only for enabling promising applications in photovoltaic devices and photochromic displays, but also for providing a useful platform for photocatalytic and photosensor units.

4.2. Increased light harvesting in photon upconversion with photonic crystals

Conventional dye-sensitized solar cells have excellent charge collection efficiencies, high open-circuit voltages and good fill factors. However, dye-sensitized solar cells do not completely absorb all of the photons from the visible and near-infrared domain and consequently have lower short-circuit photocurrent densities than inorganic photovoltaic devices. Here, we present a new design where low-energy photons are absorbed by highly photoluminescent layer of chromophores attached to the cell and

undergo energy transfer to the sensitizing dye by TTA-based upconverted emission. This architecture allows for broader spectral absorption, resulting in an increase in intensity of high-energy light which can be absorbed by the sensitizing dye. Moreover, as an optical construtive mirror, the photonic crystal structure provided for highly enhanced intensity of photons from upconverted emission, even though the transmitted photons through a solar cell were dimished. We demonstrate a 15-20% increase in power conversion efficiency when using a pair of energy upconverting relay dyes (PtPTBP and BPEA) with an organic sensitizing dye (N-719). This system offers a viable pathway to develop more efficient dye-sensitized solar cells.

4.3. Future works

Although the results presented here lead to a significant clarification of the role of photon upconverting microstructures in influencing energy transfer and harvesting, further experiments must be conducted to elucidate the fundamental photochemistry related science. In order to accomplish this in-depth goal, spectroscopic and time-resolved photoluminescence studies will significantly help understanding and developing diffusive energy transfer kinetics within multi-molecular systems at the nano- and micro-second timescales described in Chapter 1. Depending on the properties of pairs of chromophores and media, fusion characteristics of the sensitized photon upconversion could be changed and defined for providing an efficient UC platform and its practical applications.

REFERENCES

[1] de Wild, J., Meijerink, A., Rath, J. K., van Sark, W. G. J. H. M. & Schropp, R. E. I. Upconverter solar cells: materials and applications. *Energy & Environmental Science* **4**, 4835-4848 (2011).

[2] Atre, A. C. & Dionne, J. A. Realistic upconverter-enhanced solar cells with non-ideal absorption and recombination efficiencies. *Journal of Applied Physics* **110**, 034505 (2011).

[3] Shan, G.-B. & Demopoulos, G. P. Near-Infrared Sunlight Harvesting in Dye-Sensitized Solar Cells Via the Insertion of an Upconverter-TiO2 Nanocomposite Layer. *Advanced Materials* **22**, 4373-4377 (2010).

[4] Cheng, Y. Y. *et al.* Improving the light-harvesting of amorphous silicon solar cells with photochemical upconversion. *Energy & Environmental Science* **5**, 6953-6959 (2012).

[5] Singh-Rachford, T. N., Lott, J., Weder, C. & Castellano, F. N. Influence of Temperature on Low-Power Upconversion in Rubbery Polymer Blends. *Journal of the American Chemical Society* **131**, 12007-12014 (2009).

[6] Zhang, Z. *et al.* Inducing photocatalysis by visible light beyond the absorption edge: Effect of upconversion agent on the photocatalytic activity of Bi2WO6. *Applied Catalysis B: Environmental* **101**, 68-73 (2010).

[7] Qin, W., Zhang, D., Zhao, D., Wang, L. & Zheng, K. Near-infrared photocatalysis based on YF3 : Yb3+,Tm3+/TiO2 core/shell nanoparticles. *Chemical Communications* **46**, 2304-2306 (2010).

[8] Khnayzer, R. S. *et al.* Upconversion-powered photoelectrochemistry. *Chemical Communications* **48**, 209-211 (2012).

[9] Wang, F. *et al.* Simultaneous phase and size control of upconversion nanocrystals through lanthanide doping. *Nature* **463**, 1061-1065 (2010).

[10] Miteva, T., Yakutkin, V., Nelles, G. & Baluschev, S. Annihilation assisted upconversion: all-organic, flexible and transparent multicolour display. *New Journal of Physics* **10**, 103002 (2008).

[11] Liu, Q., Yang, T., Feng, W. & Li, F. Blue-Emissive Upconversion Nanoparticles for Low-Power-Excited Bioimaging in Vivo. *Journal of the American Chemical Society* **134**, 5390-5397 (2012).

[12] Lim, S. F. *et al.* In Vivo and Scanning Electron Microscopy Imaging of Upconverting Nanophosphors in Caenorhabditis elegans. *Nano Letters* **6**, 169-174 (2005).

[13] Haase, M. & Schäfer, H. Upconverting Nanoparticles. *Angewandte Chemie International Edition* **50**, 5808-5829 (2011).

[14] Wohnhaas, C. *et al.* Annihilation Upconversion in Cells by Embedding the Dye System in Polymeric Nanocapsules. *Macromolecular Bioscience* **11**, 772-778 (2011).

[15] Baluschev, S. *et al.* Blue-Green Up-Conversion: Noncoherent Excitation by NIR Light. *Angewandte Chemie International Edition* **46**, 7693-7696 (2007).

[16] Singh-Rachford, T. N. & Castellano, F. N. Photon upconversion based on sensitized triplet–triplet annihilation. *Coordination Chemistry Reviews* **254**, 2560-2573 (2010).

[17] Monguzzi, A., Tubino, R., Hoseinkhani, S., Campione, M. & Meinardi, F. Low power, non-coherent sensitized photon up-conversion: modelling and perspectives. *Physical Chemistry Chemical Physics* **14**, 4322-4332 (2012).

[18] Islangulov, R. R. & Castellano, F. N. Photochemical Upconversion: Anthracene Dimerization Sensitized to Visible Light by a RuII Chromophore. *Angewandte Chemie International Edition* **45**, 5957-5959 (2006).

[19] Ji, S., Guo, H., Wu, W., Wu, W. & Zhao, J. Ruthenium(II) Polyimine–Coumarin Dyad with Non-emissive 3IL Excited State as Sensitizer for Triplet–Triplet Annihilation Based Upconversion. *Angewandte Chemie International Edition* **50**, 8283-8286 (2011).

[20] Parker, C. A. & Hatchard, C. G. DELAYED FLUORESCENCE FROM SOLUTIONS OF ANTHRACENE AND PHENANTHRENE. *Proceedings of the Royal Society of London Series a-Mathematical and Physical Sciences* **269**, 574- (1962).

[21] Parker, C. A., Hatchard, C. G. & Joyce, T. A. Selective and Mutual Sensitization of Delayed Fluorescence. *Nature* **205**, 1282-1284 (1965).

[22] Shockley, W. & Queisser, H. J. Detailed Balance Limit of Efficiency of p-n Junction Solar Cells. *Journal of Applied Physics* **32**, 510-519 (1961).

[23] Yeh, A. T., Shank, C. V. & McCusker, J. K. Ultrafast Electron Localization Dynamics Following Photo-Induced Charge Transfer. *Science* **289**, 935-938 (2000).

[24] Islangulov, R. R., Kozlov, D. V. & Castellano, F. N. Low power upconversion using MLCT sensitizers. *Chemical Communications*, 3776-3778 (2005).
[25] Joannopoulos, J. D., Villeneuve, P. R. & Fan, S. H. Photonic crystals: Putting a new twist on light. *Nature* **386**, 143-149 (1997).

[26] Joannopoulos, J. D., Meade, R. D. & Winn, J. N. Photonic crystals: Molding the flow of light. *Princeton university press* (1995).

[27] Yablonovitch, E. INHIBITED SPONTANEOUS EMISSION IN SOLID-STATE PHYSICS AND ELECTRONICS. *Physical Review Letters* **58**, 2059-2062 (1987).

[28] John, S. STRONG LOCALIZATION OF PHOTONS IN CERTAIN DISORDERED DIELECTRIC SUPERLATTICES. *Physical Review Letters* **58**, 2486-2489 (1987).

[29] Psaltis, D., Quake, S. R. & Yang, C. H. Developing optofluidic technology through the fusion of microfluidics and optics. *Nature* **442**, 381-386 (2006).

[30] Sakoda, K. Optical properties of photonic crystals. *Springer-Verlag, Berlin* (2001).

[31] Yi, G.-R., Moon, J. H. & Yang, S.-M. Photonic Crystals for Controlling the Light. *News & Information for Chemical Engineers* **23**, 446-455 (2005).

[32] Johnson, S. G. & Joannopoulos, J. D. Introduction to Photonic Crystals: Bloch's Theorem, Band Diagrams, and Gaps (But No Defects). *Photonic Crystals Tutorial: Lecture 1* (2003).

[33] Moon, J. H. Fabrication of photonic crystals by holographic lithography. *Doctoral Thesis* (2005).

[34] Johnson, S. G. Photonic Crystals: A Crash Course in Designer Electromagnetism. *A short course at SPIE Photonics West* (2007).

[35] Monguzzi, A., Tubino, R. & Meinardi, F. Multicomponent Polymeric Film for Red to Green Low Power Sensitized Up-Conversion. *The Journal of Physical Chemistry A* **113**, 1171-1174 (2009).

[36] Mezyk, J., Tubino, R., Monguzzi, A., Mech, A. & Meinardi, F. Effect of an External Magnetic Field on the Up-Conversion Photoluminescence of Organic Films: The Role of Disorder in Triplet-Triplet Annihilation. *Physical Review Letters* **102**, 087404 (2009).

[37] Monguzzi, A., Tubino, R. & Meinardi, F. Upconversion-induced delayed fluorescence in multicomponent organic systems: Role of Dexter energy transfer. *Physical Review B* **77**, 155122 (2008).

[38] Islangulov, R. R., Lott, J., Weder, C. & Castellano, F. N. Noncoherent Low-Power Upconversion in Solid Polymer Films. *Journal of the American Chemical Society* **129**, 12652-12653 (2007).

[39] Kim, J.-H., Deng, F., Castellano, F. N. & Kim, J.-H. High Efficiency Low-Power Upconverting Soft Materials. *Chemistry of Materials* **24**, 2250-2252 (2012).

[40] Singh-Rachford, T. N. & Castellano, F. N. Triplet Sensitized Red-to-Blue Photon Upconversion. *The Journal of Physical Chemistry Letters* **1**, 195-200 (2009).

[41] Monguzzi, A., Frigoli, M., Larpent, C., Tubino, R. & Meinardi, F. Low-Power-Photon Up-Conversion in Dual-Dye-Loaded Polymer Nanoparticles. *Advanced Functional Materials* **22**, 139-143 (2012).

[42] Umbanhowar, P. B., Prasad, V. & Weitz, D. A. Monodisperse Emulsion Generation via Drop Break Off in a Coflowing Stream. *Langmuir* **16**, 347-351 (1999).

[43] Utada, A. S., Fernandez-Nieves, A., Stone, H. A. & Weitz, D. A. Dripping to Jetting Transitions in Coflowing Liquid Streams. *Physical Review Letters* **99**, 094502 (2007).

[44] Jiang, P. & McFarland, M. J. Large-Scale Fabrication of Wafer-Size Colloidal Crystals, Macroporous Polymers and Nanocomposites by Spin-Coating. *Journal of the American Chemical Society* **126**, 13778-13786 (2004).

[45] Kim, S.-H. *et al.* Optofluidic Assembly of Colloidal Photonic Crystals with Controlled Sizes, Shapes, and Structures. *Advanced Materials* **20**, 1649-1655 (2008).

[46] Kim, S.-H., Kim, S.-H., Jeong, W. C. & Yang, S.-M. Low-Threshold Lasing in 3D Dye-Doped Photonic Crystals Derived from Colloidal Self-Assemblies. *Chemistry of Materials* **21**, 4993-4999 (2009).

[47] Monguzzi, A., Tubino, R., Salamone, M. M. & Meinardi, F. Energy transfer enhancement by oxygen perturbation of spin-forbidden electronic transitions in aromatic systems. *Physical Review B* **82**, 125113 (2010).

[48] Olmsted, J. Calorimetric determinations of absolute fluorescence quantum yields. *The Journal of Physical Chemistry* **83**, 2581-2584 (1979).

[49] Wang, W., Gu, B., Liang, L. & Hamilton, W. A. Fabrication of Near-Infrared Photonic Crystals Using Highly-Monodispersed Submicrometer SiO2 Spheres. *The Journal of Physical Chemistry B* **107**, 12113-12117 (2003).

[50] Stöber, W., Fink, A. & Bohn, E. Controlled growth of monodisperse silica spheres in the micron size range. *Journal of Colloid and Interface Science* **26**, 62-69 (1968).

[51] Hench, L. L. & West, J. K. The sol-gel process. *Chemical Reviews* **90**, 33-72 (1990).

[52] Yokoi, T. *et al.* Periodic Arrangement of Silica Nanospheres Assisted by Amino Acids. *Journal of the American Chemical Society* **128**, 13664-13665 (2006).

[53] Yokoi, T. *et al.* Mechanism of Formation of Uniform-Sized Silica Nanospheres Catalyzed by Basic Amino Acids. *Chemistry of Materials* **21**, 3719-3729 (2009).

[54] Hartlen, K. D., Athanasopoulos, A. P. T. & Kitaev, V. Facile Preparation of Highly Monodisperse Small Silica Spheres (15 to >200 nm) Suitable for Colloidal Templating and Formation of Ordered Arrays. *Langmuir* **24**, 1714-1720 (2008).

[55] O'Regan, B. & Gratzel, M. A low-cost, high-efficiency solar cell based on dye-sensitized colloidal TiO2 films. *Nature* **353**, 737-740 (1991).

[56] Nazeeruddin, M. K. *et al.* Combined Experimental and DFT-TDDFT Computational Study of Photoelectrochemical Cell Ruthenium Sensitizers. *Journal of the American Chemical Society* **127**, 16835-16847 (2005).

[57] Hamann, T. W., Jensen, R. A., Martinson, A. B. F., Van Ryswyk, H. & Hupp, J. T. Advancing beyond current generation dye-sensitized solar cells. *Energy & Environmental Science* **1**, 66-78 (2008).

[58] Grätzel, M. Conversion of sunlight to electric power by nanocrystalline dye-sensitized solar cells. *Journal of Photochemistry and Photobiology A: Chemistry* **164**, 3-14 (2004).

[59] Cid, J.-J. *et al.* Molecular Cosensitization for Efficient Panchromatic Dye-Sensitized Solar Cells. *Angewandte Chemie International Edition* **46**, 8358-8362 (2007).

[60] Hardin, B. E. *et al.* Increased light harvesting in dye-sensitized solar cells with energy relay dyes. *Nat Photon* **3**, 406-411 (2009).

[61] Hardin, B. E., Snaith, H. J. & McGehee, M. D. The renaissance of dye-sensitized solar cells. *Nat Photon* **6**, 162-169 (2012).

[62] Lee, K., Park, S. W., Ko, M. J., Kim, K. & Park, N.-G. Selective positioning of organic dyes in a mesoporous inorganic oxide film. *Nat Mater* **8**, 665-671 (2009).